Surface simulation studies of the hydration of white rust Fe(OH)2, goethite α-FeO(OH) and hematite α-Fe2O3

ARTICLE *in* GEOCHIMICA ET COSMOCHIMICA ACTA · APRIL 2007

Impact Factor: 4.33 · DOI: 10.1016/j.gca.2007.01.002

2 AUTHORS:

Nora H. de Leeuw
Cardiff University
240 PUBLICATIONS **4,417** CITATIONS
SEE PROFILE

Tim G Cooper
Edanz Group Ltd.
20 PUBLICATIONS **590** CITATIONS
SEE PROFILE

Available online at www.sciencedirect.com
ScienceDirect
Geochimica et Cosmochimica Acta 71 (2007) 1655–1673
Geochimica et Cosmochimica Acta
www.elsevier.com/locate/gca

Surface simulation studies of the hydration of white rust $Fe(OH)_2$, goethite α-FeO(OH) and hematite α-Fe_2O_3

Nora H. de Leeuw [a,b,*], Timothy G. Cooper [b,1]

[a] Department of Chemistry, University College London, 20 Gordon Street, London WC1H 0AJ, UK
[b] School of Crystallography, Birkbeck College, University of London, Malet Street, London WC1E 7HX, UK

Received 3 July 2006; accepted in revised form 4 January 2007; available online 10 January 2007

Abstract

Computer modelling techniques were used to elucidate the hydration behaviour of three iron (hydr)oxide minerals at the atomic level: white rust, goethite and hematite. A potential model was first adapted and tested against the bulk structures and properties of eight different iron oxides, oxyhydroxides and hydroxides, followed by surface simulations of $Fe(OH)_2$, α-FeO(OH) and α-Fe_2O_3. The major interaction between the adsorbing water molecules and the surface is through interaction of their oxygen ions with surface iron ions, followed by hydrogen-bonding to surface oxygen ions. The energies released upon the associative adsorption of water range from 1 to 17 kJ mol^{-1} for $Fe(OH)_2$, 26 to 80 kJ mol^{-1} for goethite and 40 to 85 kJ mol^{-1} for hematite, reflecting the increasing oxidation of the iron mineral. Dissociative adsorption at goethite and hematite surfaces releases larger hydration energies, ranging from 120 to 208 kJ mol^{-1} for goethite and 76 to 190 kJ mol^{-1} for hematite.

The thermodynamic morphologies of the minerals, based on the calculated surface energies, agree well with experimental morphologies, where these are available. When the partial pressures required for adsorption of water from the gas phase are plotted against temperature for the goethite and hematite surfaces, taking into account experimental entropies for water, it appears that these minerals may well be instrumental in the retention of water during the cyclic variations in the atmosphere of Mars.

1. INTRODUCTION

Iron oxides and hydroxides play an important rôle in many disciplines including pure, environmental and industrial chemistry, soil science, and biology (Schwertmann and Cornell, 2000). Iron oxides are common in the environment, where they are beneficial as they help to regulate the concentrations of organic and inorganic pollutants. They are introduced from the earth's crust during rock weathering and are present in soils, rocks, lakes, rivers and in sea beds, with the most common form being hematite α-Fe_2O_3. Iron oxides are also used in a range of applications, including as magnetic materials (Suber et al., 2005) and catalysts (Lei et al., 2005), as well as pigments, passivating thin films (Hendy et al., 2003; Hendy et al., 2005) and environmental remediation agents (Meng et al., 2002; Zhang and Selim, 2005). In recent years, a range of novel structures have been synthesised and/or investigated for a range of purposes, for example FeO rings and clusters (Jones et al., 2005), single-crystal iron oxide nanotubes (Jia et al., 2005) and nano-sized thin films for electrochemical applications (Chung et al., 2005).

Water plays a significant rôle in many processes occurring at iron oxide surfaces, for example as a reactant in some catalytic reactions (Muhler et al., 1990), as an oxidising agent in a number of iron oxide phase transitions (Ketteler et al., 2001), in the regulation of Fe(II) and Fe(III)

* Corresponding author. Fax: +44 20 7679 7463.
E-mail address: n.h.deleeuw@ucl.ac.uk (N.H. de Leeuw).
[1] Present address: The Pfizer Institute for Pharmaceutical Materials Science, Department of Chemistry, University of Cambridge, Lensfield Road, Cambridge CB2 1EW, UK.

0016-7037/$ - see front matter © 2007 Elsevier Ltd. All rights reserved.
doi:10.1016/j.gca.2007.01.002

concentrations in living organisms (Mann et al., 1989), in the atmospheric chemistry of aerosols (Baumgärtel et al., 1999; Meskhidze et al., 2003), and possibly in the formation of iron oxide species during the Earth's accretion (Ohtani et al., 2005). Recently, the interaction of water with iron-containing minerals has gained additional attention, as explorations of the planet Mars have identified water ice and large deposits of iron (hydr)oxides (Bell et al., 2000; Morris et al., 2000), especially hematite (Christensen et al., 2000, 2006; Lane et al., 2002), indicating the presence and activity of water (Newsom et al., 2003; Chevrier et al., 2004). The evidence of both water and iron-containing minerals on Mars is of especial interest as this combination could lead to favourable conditions for pre-biotic or biotic processes involving bacteria (Robbins and Iberall, 1991; Allen et al., 2004; Edwards et al., 2004).

In view of the importance of the water/iron oxide interface, it is not surprising that it has been the topic of much research, both experimentally and computationally. For example, Leist et al. (2003) have investigated the formation of ice layers on FeO, Fe_3O_4 and Fe_2O_3 films, whereas Jolivet et al. (2004) have investigated the condensation of aqueous clusters into iron (hydr)oxides. Recent environmental studies of the rôle of water at iron oxide surfaces include the work by Baltrusaitis and Grassian (2005) on the reaction of CO_2 at the water/oxide interface, and the nucleation of ice at acid-coated iron oxide powders by Archuleta et al. (2005). Computer modelling studies have mainly concentrated on the most stable hematite phase (e.g. Wasserman et al., 1997, 1999; Parker et al., 1999; Rustad et al., 1999; Jones et al., 2000; Lado-Touriño and Tsobnang, 2000), although some recent studies have also considered the bulk goethite structure (Rosso and Rustad, 2001) and some water/goethite interfaces (Shroll and Straatsma, 2003; Kerisit et al., 2005).

One of the aims of this work was to develop and present an interatomic potential model, that can be used for both ferrous and ferric oxides and hydroxides in an aqueous environment, and that is fully transferable between the different phases. Once derived, we have tested this interatomic potential model by investigating computationally the adsorption of water at surfaces of three crystalline iron (hydr)oxide minerals: the iron oxide hematite, the iron oxyhydroxide goethite and the iron hydroxide white rust $Fe(OH)_2$. Goethite and hematite are the most thermodynamically stable iron oxides under aerobic conditions, whereas $Fe(OH)_2$, which is not as thermodynamically stable as the other two oxides, is kinetically more favourable (Schwertmann and Cornell, 2000). We have chosen these minerals, firstly because they provide all the necessary iron and oxide species of the iron (hydr)oxide phases, and secondly because they form a series of increasing dehydration of the iron oxide, from the meta-stable fully hydroxylated brucite-structured $Fe(OH)_2$ to the oxyhydroxide goethite, which further condenses into the iron oxide hematite. The Fe(III) ions in both hematite and goethite are located in octahedral sites surrounded by oxygen or hydroxy ions, which are almost hexagonally closed-packed (hcp). The α-phases of each iron oxide/hydroxide also contain tetrahedral interstices between three oxygen or hydroxy ions in one plane and those in the plane above (Schwertmann and Cornell, 2000). As already mentioned, the iron hydroxide, $Fe(OH)_2$ is less common than the other two forms and has the brucite structure, with hcp oxygen ions and Fe^{2+} ions occupying the octahedral holes. In solution it converts to other oxides and hydroxides via oxidation/dehydration/hydrolysis (Schwertmann and Cornell, 2000).

2. METHODOLOGY

The structures and energies of the dry and hydrated iron (hydr)oxide surfaces were modelled using energy minimisation techniques, based on the Born model of solids (Born and Huang, 1954), which assumes that the ions in the crystal interact *via* long-range electrostatic forces and short-range forces. In the surface calculations, the long-range Coulombic interactions are calculated using the Parry technique (Parry, 1975, 1976), whereas the short-range repulsions and Van der Waals attractions between neighbouring electron charge clouds are described by parameterised analytical expressions. The electronic polarisability of the ions is included *via* the shell model of Dick and Overhauser (1958), where each polarisable ion, in our case the oxygen ion, is represented by a core and a massless shell, connected by a spring. The polarisability of the model ion is then determined by the spring constant and the charges of the core and shell. When necessary, angle-dependent forces are included to allow directionality of bonding as, for example, in the water molecule. The energy minimisation code employed for the derivation of the potential model and the calculation of the bulk crystal properties was PARAPOCS (Parker et al., 1987), while the surfaces were modelled using the code METADISE (Watson et al., 1996), which is designed to model dislocations, interfaces and surfaces.

Tasker (1979) identified three different types of surfaces, (i) an uncharged plane with cations and anions in stoichiometric ratio, (ii) a stack of charged planes where the repeat unit perpendicular to the surface has no dipole moment, and finally (iii) a stack of charged planes where the repeat unit has a dipole moment perpendicular to the surface. In the last instance the surface needs to be reconstructed to remove the dipole, which is often achieved by creating surface vacancies. Following the approach of Tasker (1979), the crystal thus consists of a series of charged planes parallel to the surface and periodic in two dimensions. The crystal is divided into two blocks each comprising two regions, region I and region II. Region I contains those atoms near the surface, which are allowed to relax to their mechanical equilibrium, while region II contains those atoms further away, which represent the rest of the crystal and are kept fixed at their bulk equilibrium position. Inclusion of region II is necessary to ensure that the potential of an ion at the bottom of region I is modelled correctly. Both regions I and II need to be sufficiently large for the energy to converge. The bulk of the crystal is simulated by the two blocks together while the surface is represented by a single block with the top of region I as the free surface. Interfaces such as stacking faults and grain boundaries can be studied by fitting two surface blocks together in different orientations. The

energies of the blocks are essentially the sum of the energies of interaction between all atoms.

The surface energy is a measure of the thermodynamic stability of the surface, with a low positive value indicating a stable surface. The surface energy (γ) is calculated as follows:

$$\gamma = \frac{(E_s - E_b)}{A} \quad (1)$$

where E_s is the energy of the surface block, E_b the energy of the bulk crystal containing the same number of atoms as the surface block, and A is the surface area. Because of the presence of water in the environment, we also calculate the surface energies of the surfaces with a monolayer of water. Adsorption of a monolayer of water is achieved by adsorbing water molecules sequentially onto the surfaces, where the most energetically favourable configuration is used as the input for the adsorption of further water. In this study we consider only the adsorption of a full monolayer of water, where by full monolayer coverage we mean that no more adsorbate molecules can be adsorbed onto the surface without the formation of a second layer or the adsorption process becoming endothermic. It was shown in molecular dynamics studies of water adsorption at MgO surfaces (de Leeuw and Parker, 1998a), that there is a clear difference between the monolayer of water adsorbed at the mineral surface and the bulk liquid water. The presence of a monolayer adsorbed on the surface disturbs the liquid structure of bulk water, leading to a gap of low water density in between the two types of water, i.e. adsorbed at the surface and in the bulk liquid. Similar behaviour was more recently identified at calcium carbonate (Kerisit and Parker, 2004a,b) and α-quartz surfaces (Du and de Leeuw, 2006) and we thus expect it to be a general effect at ionic surfaces. Furthermore, only the adsorbed water monolayer was shown to affect the structure and energy of the underlying surface, and in this study we therefore only consider an adsorbed monolayer. As there may be a number of different stable geometries for the adsorbed water molecules, we have used a range of different starting structures in our simulations to ensure that we obtain the lowest energy configuration of the water adsorbed at the mineral surfaces (Mkhonto and de Leeuw, 2002).

The surface energies of the hydrated surfaces are defined by:

$$\gamma_{hydrated} = \frac{(E_{s+water} - nE_{water} - E_b)}{A} \quad (2)$$

where $E_{s+water}$ is the energy of the surface with adsorbed water and E_{water} is the energy of a water molecule and n is the number of water molecules adsorbed to the surface. The energy of an associatively adsorbed water molecule is made up of two parts; its self-energy, which is the energy of the gaseous molecule, calculated as an isolated water molecule, and its solvation energy, which is the energy required to remove the molecule from its hydration shell in the aqueous solution.

Calculation of the dissociative adsorption of water using interatomic potential-based methods is less straightforward. Here, the energy of dissociation of the water molecule is required as well, but this reaction requires the second electron affinity of oxygen, which is material-dependent. However, this energy can be obtained from an energy cycle using experimental enthalpies for some of the reactions, as well as lattice energies calculated in this work, as shown below:

$$\begin{array}{ccc} Fe_2O_{3(s)} + H_2O_{(l)} & \xrightarrow{\Delta H} & 2FeO(OH)_{(s)} \\ \uparrow E_{latt}\{Fe_2O_3\} & & \uparrow 2E_{latt}\{FeO(OH)\} \\ 2Fe^{3+} + 3O^{2-} + H_2O_{(l)} & \xrightarrow{E_{H2O}} & 2Fe^{3+} + 2\,O^{2-} + 2OH^- \end{array} \quad (3)\ (4)$$

where ΔH is the experimental enthalpy of reaction (3) (Lide, 2000; Majzlan et al., 2003), which was found to be -6.3 kJ mol^{-1}, $E_{latt}\{FeO(OH)\}$ and $E_{latt}\{Fe_2O_3\}$ are the calculated lattice energies of FeO(OH) and Fe_2O_3, which were calculated to be -6917.7 and -14510.6 kJ mol^{-1}, respectively. This energy cycle is used to obtain the energy of the reaction of one surface oxygen ion with one water molecule to form two hydroxy groups:

$$O^{2-} + H_2O_{(l)} \xrightarrow{E_{H_2O}} 2OH^- \quad (5)$$

which is calculated at $E_{H_2O} = -681.4$ kJ mol^{-1}. This energy, which represents the energy for the dissociation of one water molecule, is used to calculate the energy released (per water molecule) upon adsorption of dissociative water at the iron (hydr)oxide surfaces as follows:

$$\begin{array}{ccc} Fe_{2x}O_{3x(surface)} + H_2O_{(l)} & \xrightarrow{E_{hydration}} & Fe_{2x}O_{3x\text{-}1}(OH)_{2(surface)} \\ \uparrow E_{latt}\{Fe_{2x}O_{3x(surface)}\} & & \uparrow E_{latt}\{Fe_{2x}O_{3x\text{-}1}(OH)_{2\,(surface)}\} \\ 2xFe^{3+} + 3xO^{2-} + H_2O_{(l)} & \xrightarrow{E_{H2O}} & 2xFe^{3+} + (3x\text{-}1)O^{2-} + 2OH^- \end{array} \quad (6)$$

where $E_{latt}\{Fe_{2x}O_{3x(surface)}\}$ is the energy of the dehydrated surface (shown here for hematite) obtained from the simulations, $E_{latt}\{Fe_{2x}O_{3x-1}(OH)_{2(surface)}\}$ is the energy of the hydroxylated surface, also obtained from the simulations, and E_{H_2O} is the energy of dissociation of one water molecule obtained from 5 above. The hydration energy of dissociative adsorption of water at the surface is thus obtained for each surface configuration directly from this energy cycle (6).

2.1. Potential model

Table 1 lists the potential parameters used in this work. We have used the interatomic potential parameters for oxygen, Fe(II) and Fe(III) ions from Lewis and Catlow (1985), together with the polarisable hydroxy potential by Baram

Table 1
Interatomic potential used in this work (short-range cutoff 20 Å)

Interaction	Charges (e)		Core–shell interaction (eV Å^{-2})
Ion	Core	Shell	
Fe(II)	+2.00		
Fe(III)	+3.00		
H (hydroxy hydrogen)	+0.40		
Hw (water hydrogen)	+0.40		
O (oxygen)	+1.00	−3.00	60.78000
Oh (hydroxy oxygen)	+0.90	−2.30	74.92038
Ow (water oxygen)	+1.25	−2.05	209.4496
	Buckingham potential		
Inter-molecular	A (eV)	ρ (Å)	C (eV Å^6)
Fe^{2+}–O^{2-}	694.10	0.3399	0.0
Fe^{2+}–$Oh^{1.4-}$	485.90	0.3399	0.0
Fe^{2+}–$Ow^{0.8-}$	277.64	0.3399	0.0
Fe^{3+}–O^{2-}	1102.40	0.3299	0.0
Fe^{3+}–$Oh^{1.4-}$	771.70	0.3299	0.0
Fe^{3+}–$Ow^{0.8-}$	441.00	0.3299	0.0
O^{2-}–O^{2-}	22764.0	0.1490	27.88
O^{2-}–$Oh^{1.4-}$	22764.0	0.1490	13.94
O^{2-}–$Ow^{0.8-}$	22764.0	0.1490	28.92
$Oh^{1.4-}$–$Oh^{1.4-}$	22764.0	0.1490	6.97
$Oh^{1.4-}$–$Ow^{0.8-}$	22764.0	0.1490	17.14
$H^{0.4+}$–O^{2-}	396.27	0.2500	0.0
$H^{0.4+}$–$Oh^{1.4-}$	311.97	0.2500	0.0
$H^{0.4+}$–$Ow^{0.8-}$	396.27	0.2500	0.0
$Hw^{0.4+}$–O^{2-}	396.27	0.2500	0.0
$Hw^{0.4+}$–$Oh^{1.4-}$	311.97	0.2500	0.0
$Hw^{0.4+}$–$Ow^{0.8-}$	396.27	0.2500	10.0
	Lennard–Jones potential		
	A (eV Å^{12})		B (eV Å^6)
$Ow^{0.8-}$–$Ow^{0.8-}$	39344.98		42.15
	Morse potential		
Intra-molecular	D (eV)	α (Å^{-1})	r_0 (Å)
$H^{0.4+} - Oh^{1.4-}_{shell}$	7.052500	3.17490	0.92580
$Hw^{0.4+} - Ow^{0.8-}_{shell}$	6.203713	2.22003	0.92376
	Three-body potential		
	K (eV rad^{-2})	Θ_0	
$Hw^{0.4+} - Ow^{0.8-}_{shell} - Hw^{0.4+}$	4.19978	108.693195	
	Intra-molecular coulombic interaction (%)		
$H^{0.4+}$–$Oh^{1.4-}$	0		
$Hw^{0.4+}$–$Ow^{0.8-}$	50		
$Hw^{0.4+}$–$Hw^{0.4+}$	50		

and Parker (1996) and the water potential by de Leeuw and Parker (1998a), as the basis of our potential model. We then derived the short-range interactions between the two iron species and the hydroxy and water oxygen ions, following the method by Schröder et al. (1992), and further refined these by fitting to eight known iron oxide, oxyhydroxide and hydroxide mineral structures (Fletcher et al., 1996). The calculated structural properties of these minerals, using the potential listed in Table 1, are compared with the experimental data in Table 2, where we have used the structure of an ordered low-temperature Fe_3O_4 phase, which at higher temperatures is disordered as to the Fe(II) and Fe(III) positions. Whereas some individual calculated values are not as close to their experimental counterparts as we would desire if we were fitting potentials to a single structure, all the ratios of internal unit cell parameters c/a are reproduced quite accurately, and taking into account the number of different structures that the single potential model has reproduced, we consider that the accuracy and transferability of the potential model is acceptable. In addition, Table 3 lists the experimental and calculated atomic coordinates of the three minerals under investigation and again, the agreement is excellent, especially taking into account that no symmetry requirements were imposed and all species within the simulation cell, as well as the cell itself, were free to move during the minimization.

The potential parameters used for the intra- and intermolecular water interactions are those described in a

Table 2
Calculated and experimental structural properties of iron (hydr)oxides

Mineral	Simulation				Experiment			
	a	*b*	*c*	*c*/*a*	*a*	*b*	*c*	*c*/*a*
FeO[A]	4.301	4.301	4.301	1.00	4.326	4.326	4.326	1.00
α-Fe_2O_3 hematite[B]	5.06	5.06	13.38	2.64	5.04	5.04	13.75	2.73
ε-Fe_2O_3[C]	5.119	8.704	9.392	1.83	5.095	8.789	9.437	1.85
Fe_3O_4 (ordered low T)[D]	5.984	5.984	16.926	2.83	5.934	5.926	16.752	2.82
α-FeO(OH) goethite[E]	4.68	9.58	3.11	0.66	4.62	9.96	3.02	0.65
β-FeO(OH)[F]	4.90	4.45	3.01	0.61	4.94	4.43	2.99	0.61
γ-FeO(OH) lepidocrocite[G]	2.95	14.07	3.89	1.32	3.08	12.5	3.87	1.26
$Fe(OH)_2$[H]	3.20	3.20	4.80	1.50	3.26	3.26	4.60	1.41

[A] Fjellvag et al. (1996).
[B] Cox et al. (1962).
[C] Tronc et al. (1998).
[D] Iizumi et al. (1982).
[E] Hazemann et al. (1992).
[F] Christensen et al. (1976).
[G] Zhukhlistov (2001).
[H] Lutz et al. (1994).

Table 3
Calculated and experimental coordinates of white rust, goethite and hematite

Mineral	Species	Experiment			Simulation		
		x	*y*	*z*	*x*	*y*	*z*
$Fe(OH)_2$[a]	Fe(II)	0.000	0.000	0.000	0.000	0.000	0.000
	O	0.3333	0.6667	0.2000	0.3333	0.6667	0.1977
	H	0.3333	0.6667	0.4000	0.3333	0.6667	0.4077
α-FeO(OH)[b]	Fe(III)	0.8554	0.2500	0.0451	0.8453	0.2500	0.0479
	Ox	0.1989	0.2500	0.7120	0.2066	0.2500	0.7417
	Oh	0.0532	0.2500	0.1970	0.0490	0.2500	0.1677
	H	0.0876	0.2500	0.4095	0.0638	0.2500	0.3807
α-Fe_2O_3[c]	Fe(III)	0.0000	0.0000	0.0000	0.0000	0.0000	0.3611
	O	0.3060	0.0000	0.2500	0.2948	0.0000	0.2500

[a] Parise et al. (2000).
[b] Hazemann et al. (1992).
[c] Cox et al. (1962).

previous study of molecular dynamics (MD) simulations on MgO surfaces (de Leeuw and Parker, 1998a); where the intra-molecular interactions between oxygen and hydrogen atoms are described by a Morse potential and the intermolecular interactions by a Buckingham potential. The steric effect that the electron lone pairs on the oxygen atom have on the geometry of the water molecule was included by partially removing the electrostatic interactions between the two hydrogen atoms and between hydrogen and oxygen atoms in the water molecule (by half), making the hydrogen atoms less repulsive, much as electrostatic interactions within organic molecules are routinely removed in potential models for biological applications. The potential model adequately describes the bulk properties of liquid water. The calculated O–O, O–H and H–H radial distribution functions agree well with experiment, both as to position and to height of the peaks (Soper and Phillips, 1986), while the calculated energy of vaporisation of 43.0 kJ mol^{-1} is in excellent agreement with the experimental value of 44.0 kJ mol^{-1} (Lide, 2000), showing that we can be confident that the energetics of binding and hydrogen-bonding are reliable, which is also important for the mineral hydration processes.

For the interactions between water molecules and the iron oxyhydroxides, we have used the potential parameters previously fitted to MgO and CaO for the O–water interactions (de Leeuw et al., 1996), which have been shown to give good quantitative agreement with experimental temperature programmed desorption data (Fubini et al., 1989; de Leeuw et al., 1996). The Fe-water interactions were derived according to the Schröder method for scaling interatomic potential parameters (Schröder et al., 1992). This approach has already been used in a variety of earlier mineral/water simulations, including quartz (de Leeuw et al., 1999, 2003), forsterite (de Leeuw et al., 2000) and calcium carbonates (de Leeuw and Parker, 1997, 1998b). The findings of these studies agree well with experimental results, especially the latter studies on calcium carbonates, where the simula-

tions reproduced and predicted surface and adsorption features in excellent agreement with experimental studies by Liang et al. (1996) and later confirmed by Fenter et al. (2000).

Finally, in previous work we have reported a number of studies of different water/mineral systems, where we have compared simulations using interatomic potentials thus derived with density functional theory (DFT) calculations. In all cases, these methods have given excellent agreement both as to adsorption geometries of the surface and water molecules as well as to adsorption energies. For example, combined studies of water adsorption at the CaF_2 {111} surface and different terminations of the {0001} surface of quartz have shown the same mode of adsorption, i.e. associative or dissociative, the same geometry of the adsorbed water molecules at the surface and the same hydration energy for both methods to within 12 kJ mol^{-1}, which is a very good agreement taking into account the approximations used in both techniques (de Leeuw and Cooper, 2003; Du and de Leeuw, 2004). A combined DFT and interatomic potential study of the layering of scheelite due to the presence of water in the bulk mineral once again showed the same result for both methods, including hydrogen-bonding across the interlayer spacing in the mineral and strength of hydration (Cooper and de Leeuw, 2003). In view of the above, we are confident that the interatomic potential derived here for the iron (hydr)oxide systems and their interaction with water will be appropriate for the calculation of the surface structures and stabilities and the adsorption energies of the hydrated white rust, goethite and hematite surfaces.

2.2. Morphologies

The equilibrium morphology of a crystal is determined by the surface energy and the related growth rate of the various surfaces and provides a measure of the relative stabilities of the surfaces. Wulf's Theorem (1901) proposed that a polar plot of surface energy versus orientation of normal vectors would give the crystal morphology based on the approach of Gibbs (1928), who proposed that under thermodynamic control the equilibrium form of a crystal should possess minimal total surface free energy for a given volume. Moreover, a surface with a high surface free energy is expected to have a large growth rate and this fast growing surface will not be expressed in the morphology of the resulting crystal. Only surfaces with low surface free energies and hence slow growing will be expressed. Molecular and lattice dynamics simulations have shown that the contribution of the excess entropy term to the surface free energy in ionic solids is small compared to the enthalpy term, as the differences between the entropies of the bulk and the surface are small (Taylor et al., 1999). In addition, although Mulheran showed that the change in surface free energy with temperature may be significant (Mulheran, 1993), Allan and coworkers calculated that this change is similar for different surfaces (Taylor et al., 1999; Allan et al., 2000). Hence, for ionic solid surfaces the surface energies are good approximations for the surface free energies, especially taking into account that in morphology calculations only the relative values of the surface free energies of the different faces are important. Thus, the surface energies can be assumed to determine the equilibrium morphology of the crystal and indeed the prediction of morphologies of even complex oxides on the basis of static surface energies has been shown in the past to successfully reproduce experimental morphologies (Parker et al., 1993; Titiloye et al., 1993; Cooper and de Leeuw, 2006).

However, crystal growth is a complex kinetic process and will be affected by many factors and hence the equilibrium morphologies should be treated more as a representation of the effect of the addition of water to the different surfaces rather than the definitive growth morphology. However, previous simulations of, for example, forsterite Mg_2SiO_4 and scheelite $CaWO_4$ have shown excellent agreement between experimental and calculated morphologies of these materials, once surface-adsorbed water was taken into account (de Leeuw et al., 2000; Cooper and de Leeuw, 2003).

3. RESULTS AND DISCUSSION

We have used the relaxed structure of hematite, goethite and $Fe(OH)_2$, obtained by optimization of their bulk structure, to create the surfaces with the desired orientation. For hematite and goethite, these surfaces were then hydrated through both dissociative and associative adsorption of a monolayer of water. We considered that a monolayer of dissociative water was obtained when all surface cations had been terminated by hydroxy groups and all surface oxygens had been protonated. For the sake of completeness, a further layer of molecular water was added to interact with the hydroxy groups at the mineral surfaces. This second water layer, adsorbed to the hydroxylated surface, already has the main characteristics of bulk water (Du and de Leeuw, 2006) and we therefore did not hydrate the surfaces any further. This water layer adsorbed to the surface hydroxy groups interacts only weakly through hydrogen-bonded interactions, and the resulting hydration energies range between 6 and 50 kJ mol^{-1}, depending on the number and strength of hydrogen bonds formed. As all oxygen ions of $Fe(OH)_2$ are already bound in hydroxy groups, only associative adsorption of water was considered at the $Fe(OH)_2$ surfaces. The calculated surface energies of all dry, hydrated and hydroxylated surfaces for all the minerals studied in this work, as well as the corresponding hydration energies, are reported in Tables 4–9.

Table 4
Calculated surface energies of pure and hydrated $Fe(OH)_2$

Surface	γ_{pure} (J m^{-2})	$\gamma_{hydrated}$ (J m^{-2})
{001}	0.05	0.02
{010} ≡ {100}	0.39	0.13
{011}	0.36	0.19
{110}	0.64	0.38
{101}	0.36	0.17
{111}	0.60	0.21

Table 5
Calculated average hydration energies of $Fe(OH)_2$ (kJ mol^{-1})

Surface	E_{hydr}
{001}	−1.3
{010} ≡ {100}	−11.8
{011}	−8.9
{110}	−13.9
{101}	−7.8
{111}	−16.6

Table 6
Calculated surface energies of pure, hydrated and hydroxylated goethite (J m^{-2})

Surface	γ_{pure}	$\gamma_{associative}$	$\gamma_{dissociative}$
{001}	1.68	1.08	0.64
{100}	1.92	0.97	0.76
{010}	0.68	0.38	1.03
{011}	1.72	1.10	0.77
{110}	1.18	0.66	0.50
{101}	1.26	1.10	0.43
{111}	1.33	0.68	0.60

Table 7
Calculated average hydration energies of goethite (kJ mol^{-1})

Surface	$E_{associative}$	$E_{dissociative}$
{001}	−80.2	−140.2
{100}	−56.5	−207.3
{010}	−25.9	+30.8
{011}	−58.4	−134.0
{110}	−34.6	−135.7
{101}	−26.3	−134.5
{111}	−43.7	−122.5

Table 8
Calculated surface energies of pure, hydrated and hydroxylated hematite (J m^{-2})

Surface	γ_{pure}	$\gamma_{associative}$	$\gamma_{dissociative}$
{0001}Fe	1.78	1.12	1.21
{0001}Ox	2.63	1.84	0.51
$\{10\bar{1}0\} \equiv \{01\bar{1}0\}$	1.99	1.60	1.01
$\{10\bar{1}1\}$	2.34	1.75	0.67
$\{01\bar{1}1\}$	2.41	1.53	0.83
$\{11\bar{2}0\}$	2.03	1.30	0.81
$\{01\bar{1}2\}$	1.88	1.13	0.97
$\{10\bar{1}2\}$	2.36	1.51	0.97
$\{11\bar{2}1\}a$	1.93	1.31	0.94
$\{11\bar{2}1\}b$	2.07	1.48	0.84

a and *b* refer to two different terminations of the same surface.

3.1. $Fe(OH)_2$

We first investigated iron(II) hydroxide, or white rust, which is a layered material with spacegroup $P\bar{3}m1$, shown in Fig. 1(a), that can be precipitated from solution in the presence of an oxidizing agent. However, it is a metastable compound, which quickly further oxides to green rust $Fe(II)_{1-2x}Fe(III)_{2x}(OH)_2{\cdot}(SO_4)_x$, a similar material where some of the Fe(II) have been oxidized to Fe(III). Charge balance is maintained by the inclusion of intercalated anions in the layered structure, for example SO_4^{2-} groups (Stipp, private communication), which keep the layers together. Natta (1928) determined the positions of the heavy ions in the $Fe(OH)_2$ structure, but not the positions of the hydrogen atoms. However, as $Fe(OH)_2$ is isostructural with brucite $Mg(OH)_2$, we have used the hydrogen positions from the brucite structure refined by Cerny et al. (1995), together with the lattice parameters of Natta (1928), as the starting structure for our geometry optimization of the bulk material, before creating and modelling the low-index {001}, {100} ≡ {010}, {011}, {110}, {101} and {111} surfaces. The calculated structure compares well with the experimental structure refined by Parise et al. (2000) for brucite-structured deuterated white rust $Fe(OH_{0.86}D_{0.14})_2$, with the interatomic distances within and between the different layers reproduced to within a few percent of their experimental values.

Table 9
Calculated average hydration energies of hematite (kJ mol^{-1})

Surface	$E_{associative}$	$E_{dissociative}$
{0001}Fe	−44.1	−75.8
{0001}Ox	−70.4	−189.0
$\{10\bar{1}0\} \equiv \{01\bar{1}0\}$	−40.3	−80.5
$\{10\bar{1}1\}$	−83.9	−119.3
$\{01\bar{1}1\}$	−75.9	−135.5
$\{11\bar{2}0\}$	−84.9	−107.0
$\{01\bar{1}2\}$	−60.2	−87.9
$\{10\bar{1}2\}$	−69.0	−112.9
$\{11\bar{2}1\}a$	−49.3	−79.1
$\{11\bar{2}1\}b$	−47.1	−97.8

a and *b* refer to two different terminations of the same surface.

The calculated surface energies of these surfaces, listed in Table 4, show that the {001} surface is by far the most stable of the surfaces studied. This considerable stability is due to the fact that this surface is already naturally present in the structure, as the top/bottom of the $Fe(OH)_2$ layers, which are stacked in the *c*-direction of the crystal (Fig. 1a). Upon further hydration by molecular water, the surface energy becomes even smaller, suggesting that cleavage of the crystal exposing the {001} surface is thermodynamically feasible. In fact, even in the bulk mineral we could expect water to become intercalated between the layers in the [001] direction, because each layer is terminated on both sides by OH groups, which repel neighboring layers, and intercalated water molecules or other polar or charged species could neutralize the opposing charges between the layers and bind them together more closely. Indeed, the main difference between white rust and green rust, is the presence of intercalated charged species between the layers, which increase the stability of the structure of green rust compared to that of white rust. As such, it is not surprising that the {001} surface is very stable and hence easily cleaved, which also agrees to some extent with the difficulty found experimentally to synthesize crystals of this compound.

Apart from the {001} surface, the stability of the {111} surface is affected most by hydration (Table 4). In Fig. 2(a),

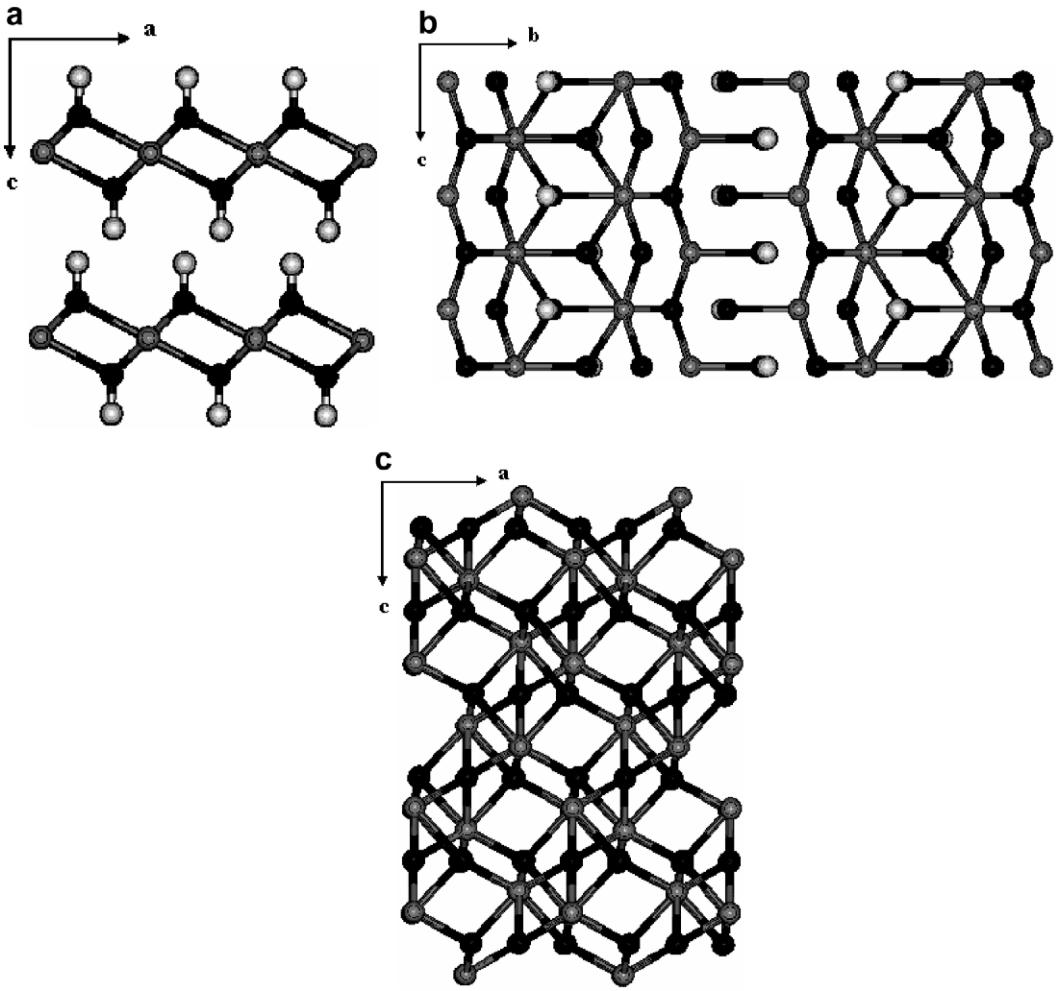

Fig. 1. Crystal structures of (a) iron hydroxide $Fe(OH)_2$, (b) goethite FeO(OH) and (c) hematite Fe_2O_3 (Fe, grey; O, black; H, white).

which illustrates the structure of the hydrated {111} surface for $Fe(OH)_2$, the topmost surface hydroxy group has relaxed away from the surface, to interact with the adsorbed water molecules. Two of these adsorbed water molecules interact strongly with the Fe(II) ion nearest the surface, at Fe–Ow distances of 2.15 and 2.20 Å, whereas the surface hydroxy groups and the adsorbed water molecules are all connected in a network of hydrogen-bonded interactions, where the major interactions are shown in Fig. 2(a), leading to a very stable, energetically favourable surface structure.

Two further surfaces, equivalent by symmetry, which are highly stabilized by the adsorption of water are the {010} and {100} surfaces, which are identical due to the crystal structure of $Fe(OH)_2$. The interesting feature of these surfaces is that they contain highly exposed Fe(II) ions at the surface and we could therefore expect a stronger interaction with the water molecules than at the {001} surface, where the water molecules are only interacting with the surface hydroxy groups through weak hydrogen-bonding (O–H > 2.4 Å). The hydration energies listed in Table 5, indeed show a stronger interaction with the {010}/{100} surfaces, but not as strong as with the {111} surface described above. Fig. 2(b) helps to explain this result; on the {010}/{100} surface, only one water molecule interacts with each surface Fe(II) ion. The geometry of the surface hydroxy groups prevents the attachment of a second water molecule to the Fe(II) ions, which did however occur on the {111} surface (Fig. 2(a) above). Interestingly, the water molecule is approximately located in a position, which corresponds roughly to the location of the hydroxy group in the bulk mineral, with Fe–Ow and O–Ow distances similar to the Fe–O and O–O distances in the $Fe(OH)_2$ structure itself (Fig. 2(b)). Similar to the {111} surface, the water molecules and surface hydroxy groups again form a network of hydrogen-bonded interactions which stabilizes both the surface and the water layer.

Considering the hydration energies listed in Table 5, we can see that there appears to be a trend in the energies. For example, on the {001} surface, water interacts with the surface only through long and weak hydrogen-bonding, releasing a negligible hydration energy (1.3 kJ mol^{-1}). On the {010} and {100} surfaces, the Fe(II) ions interact with the oxygen of one water molecule each, releasing an average hydration energy of 11.8 kJ mol^{-1}, whereas two water molecules each interact with the iron ions in the {111} surface, releasing a hydration energy of 16.6 kJ mol^{-1}. To see whether this was trend was more general, we also analysed the structures of the {011}, {110} and {101} surfaces. As

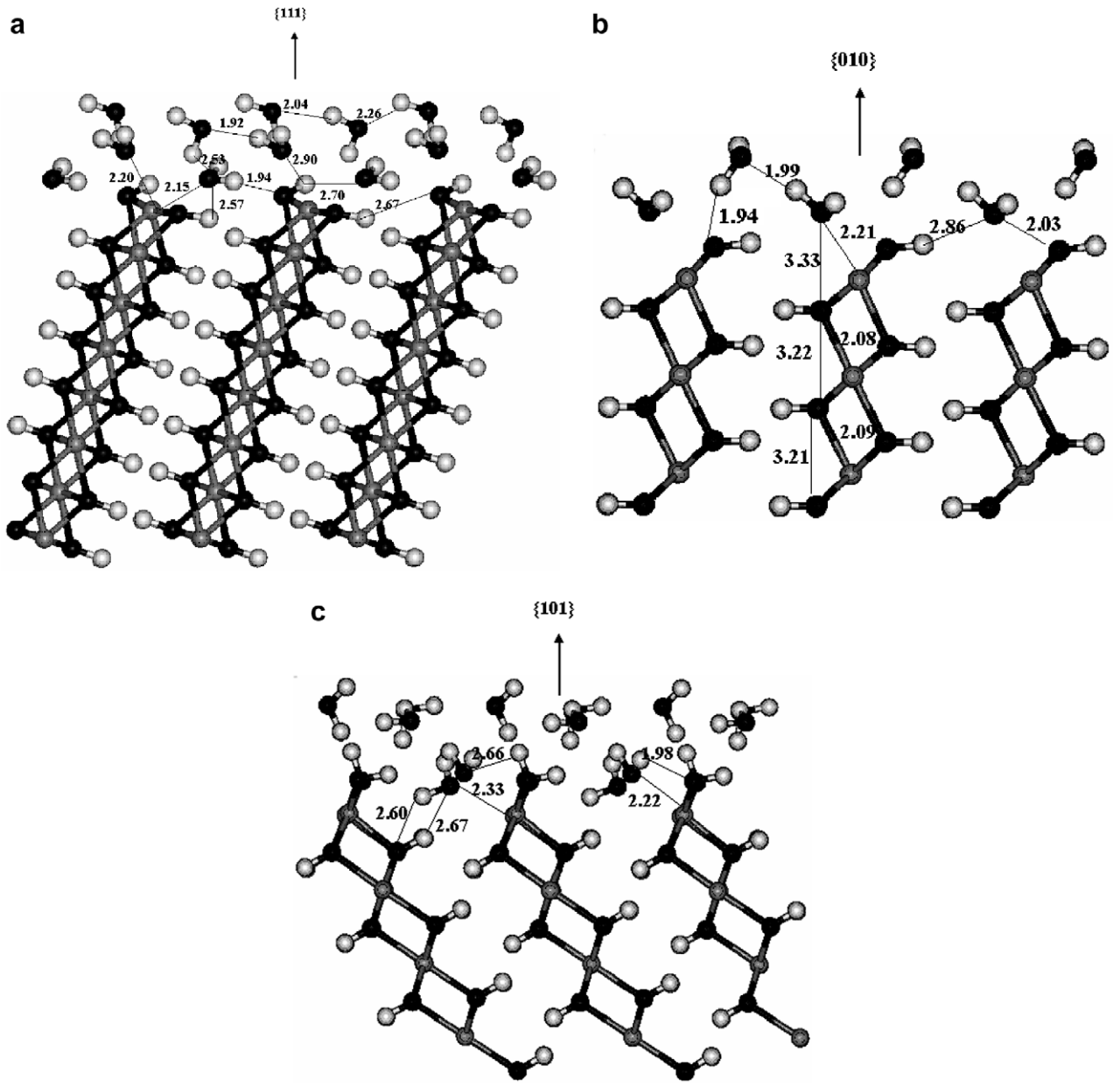

Fig. 2. Geometry-optimized structures of hydrated $Fe(OH)_2$ surfaces: (a) the {111} surface, (b) the {010} or {100} surface and (c) the {101} surface (Fe, grey; O, black; H, white, distances shown in Å).

could be expected from the hydration energies, the Fe(II) ions in the {011} surface coordinate to only one water molecule each, whereas the Fe(II) ions in the {110} surface each interact closely with two water molecules. However, the {101} is a less straightforward case; although only one water molecule interacts with each Fe(II) ion (two for each Fe(II) ion per simulation cell), these water molecules have become adsorbed in surface vacancies at locations corresponding to the position of the hydroxyl groups in the bulk material, thus establishing close interactions with the surface iron and hydroxy ions and smoothing the surface, as shown in Fig. 2(c). This type of adsorption at surface vacancies, leading to close surface-adsorbate coordination and smoothing of an otherwise irregular surface has been shown on other materials to lead to large hydration energies, for example MgO, Al_2O_3 and $CaWO_4$ (de Leeuw et al., 1996; de Leeuw and Parker, 1999; Cooper and de Leeuw, 2003). Due to their adsorption at these reactive sites, these two water molecules, releasing an adsorption energy of 13.5 kJ mol^{-1} each, largely determine the hydration energy. The remaining three water molecules per simulation cell only account for the release of a further 4.00 kJ mol^{-1} each through the formation of a network of hydrogen-bonded interactions with the surface hydroxy groups and other water molecules. This interaction is much weaker than adsorption to surface Fe(II) ions, first because protons are much less highly charged than the Fe(II) ions and the latter's interaction with the oxygen of a water molecule is therefore stronger. Second, the hydration energy is the energy difference per water molecule between being

adsorbed at the surface and being coordinated to other water molecules in a liquid water environment. As the interaction with surface hydroxy groups is similar to the interaction with other liquid water molecules, hydrogen-bonding to surface hydroxy groups only, rather than interaction with the more highly charged Fe(II) species, will be energetically more or less neutral, as is shown for the hydration of the {001} surface, where only hydroxy groups are present for interaction with the water molecules.

The final contribution to the hydration energy is the effect of hydration on the surface structure and stability. When an unstable surface is hydrated, its relaxed structure is usually more bulk-like than the dehydrated and often highly reconstructed plane, as the under-coordinated surface ions become coordinated by water molecules. As a result, the energy difference between the dehydrated and hydrated surfaces is large, leading to high hydration energies, whereas a more stable dehydrated surface, which does not undergo significant relaxation with respect to the bulk mineral, will be less affected by water molecules leading to modest hydration energies. These effects are clearly surface dependent and cannot be deduced from the number of Fe–Ow interactions.

3.2. Goethite α-FeO(OH)

Further oxidation of Fe(II) hydroxides eventually leads to the formation of goethite, α-FeO(OH), which has an orthorhombic structure with the *Pbnm* space group. We have used the structure refined by Hazemann et al. (1992) as our starting structure and after geometry optimisation of the bulk structure, we have created and modelled the low-index {100}, {001}, {010}, {101}, {011}, {110} and {111} surfaces. All surfaces were then hydrated by associative and dissociative adsorption of water molecules and the calculated surface energies for the different surfaces are listed in Table 6.

One of the dominant goethite surfaces is the {010} surface (Deer et al., 1992), which is calculated to be by far the most stable surface, both dehydrated and when hydrated by a monolayer of associated water molecules. Unlike the other goethite surfaces, its surface energy increases on dissociative adsorption of water (Table 6) with a positive hydration energy (Table 7), i.e. it is energetically unfavourable for a liquid water molecule to become dissociatively adsorbed at this surface. Fig. 3 shows the {010} surface before and after associative and dissociative adsorption of water, and the hydroxylated structure after adsorption of another layer of water molecules. Although the presence of this extra water layer stabilizes the hydroxylated surface to some extent ($\gamma = 0.85$ J m^{-2}), it is still not as stable as the surface hydrated by molecular water only ($\gamma = 0.38$ J m^{-2}), which is shown in Fig. 3(b). The reason for the preference for associative adsorption at the goethite {010} surface is structural. Although the Fe(III) ion at the surface is under-coordinated (bonded to five oxygen ions) with respect to its bulk-coordination of six, the topmost oxygen ions (not those of the hydroxy groups) are both in their full bulk-coordination of three. As such, associative adsorption of water will complete the coordination shell of the surface Fe(III) ion, and stabilize the surface through a network of hydrogen-bonded interactions to the surface oxygen ions and hydroxy groups, as shown in Fig. 3(b). On the other hand, dissociative adsorption of water leads to the addition of a proton to one of the surface oxygen ions, hence over-coordinating this oxygen ion with respect to its bulk coordination. In addition, the higher rigidity of the hydroxylated surface due to the added hydroxy groups now chemically bonded to the surface Fe(III) ion, leads to a decrease in hydrogen-bonded interactions between the existing hydroxy-groups of the surface and the dissociated water molecule, shown in Fig. 3(c). Even when another water layer is added to the hydroxylated surface, shown in Fig. 3(d), the dissociative adsorption energy remains positive ($E_{\text{hydroxylated}} = +29.8$ kJ mol^{-1}) as the surface oxygen ion is still over-coordinated with respect to the bulk. In addition, the interaction of the additional water molecules has little or no effect on the hydration energy, because the interaction of water with a hydroxylated surface is similar to the interaction of water molecules in liquid water (Du and de Leeuw, 2006).

The {010} surface is the only goethite surface considered here that has the full bulk-coordination of its surface oxygen ions, which is probably why this is the perfect cleavage plane of goethite (Deer et al., 1992). The other goethite surfaces considered in this study have surface oxygen ions with a coordination number of two, and they also often contain four-coordinated surface Fe(III) ions, for example on the {001}, {100}, {011} and {111} surfaces. Dissociative adsorption of water, which both completes the coordination of the surface oxygen ions as well as increases the coordination of the under-coordinated Fe(III) surface ion, is therefore favoured over associative adsorption at all of these surfaces (Table 7) and all surfaces are also stabilized by hydroxylation (Table 6). Kerisit et al., 2005 have investigated hydration of the goethite {100} surface by molecular dynamics simulations, although they have not considered dissociative adsorption of water at the surface, only associative adsorption. However, the adsorption pattern of molecular water from their simulations agrees with our calculations.

3.3. Hematite α-Fe_2O_3

Finally, further dehydration of goethite leads to formation of hematite, α-Fe_2O_3 (e.g. Loffler and Mader, 2006), which has a hexagonal structure with space group $R\bar{3}c$ (Cox et al., 1962). The oxygen ions are approximately in a hexagonal close-packing arrangement, where the Fe(III) ions are located between the O layers and octahedrally coordinated to six O atoms (Fig. 1(c)). Hematite is isostructural with corundum (α-Al_2O_3) and cromia (α-Cr_2O_3), which have been studied extensively, both by means of atomistic simulation techniques and experimentally (e.g. Catlow et al., 1982; Mackrodt et al., 1987; Gillet and Ealet, 1992; Guo et al., 1992; Wang, 1992; Ching and Xu, 1994; Kim et al., 1994; Rohr et al., 1997; de Leeuw and Parker, 1999). In these materials, the {0001} surface has been shown to be particularly dominant (e.g. Mackrodt, 1992; Coustet and Jupille, 1994; Godin and LaFemina, 1994;

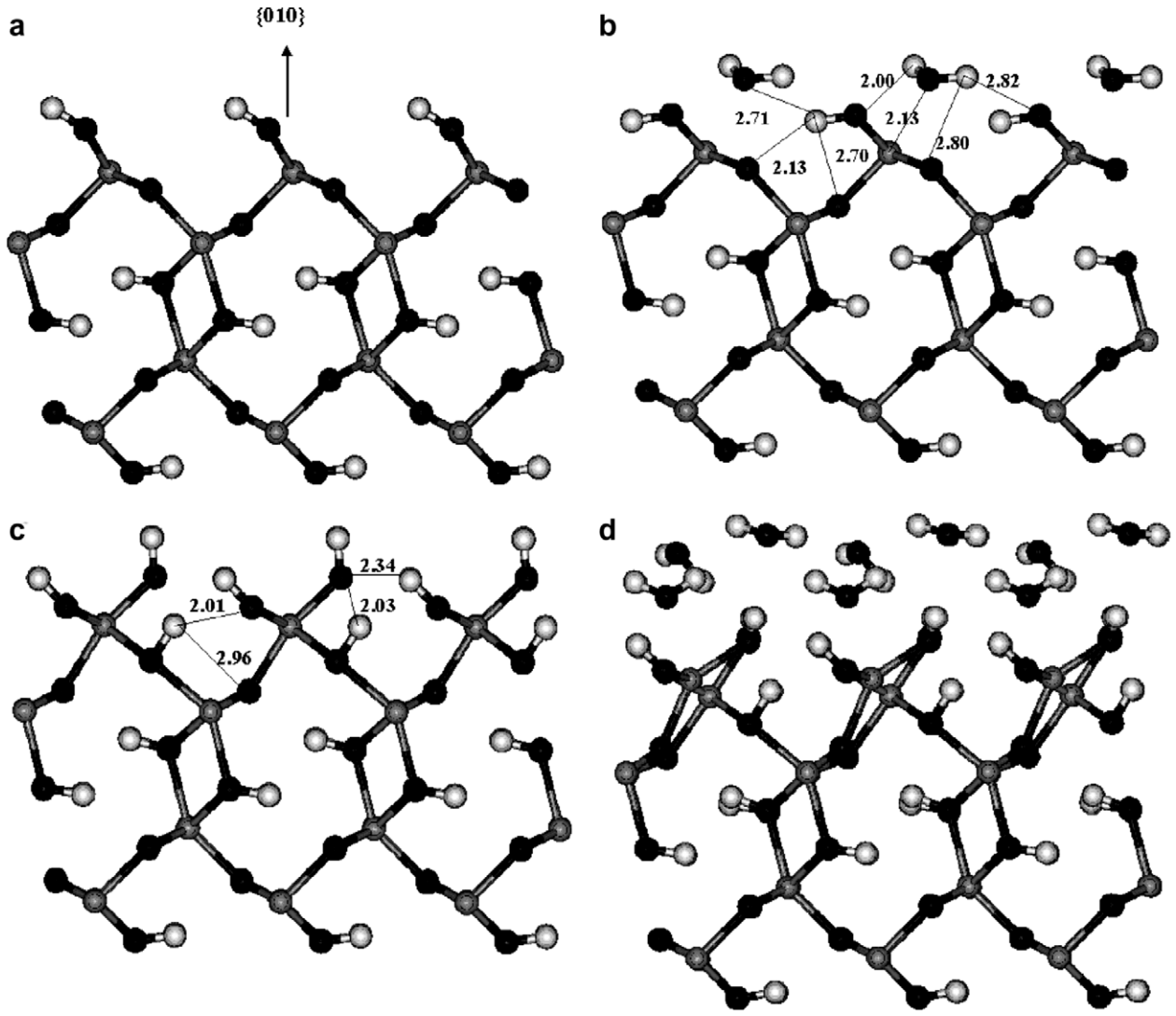

Fig. 3. Geometry-optimized goethite {010} surfaces, showing the surface (a) before hydration, (b) after associative adsorption of water, (c) after dissociative adsorption of water and (d) after adsorption of a layer of molecular water to the hydroxylated surface (Fe, grey; O, black; H, white; distances shown in Å).

Manassidis and Gillan, 1994; Nygren et al., 1997; de Leeuw and Parker, 1999) and this plane is therefore one of the surfaces studied in this work as well. In addition, we have also investigated the $\{10\bar{1}0\} \equiv \{01\bar{1}0\}$, $\{10\bar{1}1\}$, $\{01\bar{1}1\}$, $\{11\bar{2}0\}$, $\{01\bar{1}2\}$, $\{10\bar{1}2\}$ and $\{11\bar{2}1\}$ surfaces, which are all experimentally important surfaces.

The {0001} surface can be terminated by either a single or double Fe(III) layer or by oxygen ions (Trainor et al., 2004). However, the double Fe-termination and the oxygen-terminated surface are dipolar. As such, only the non-polar single Fe-termination will be considered further and in order to remove the dipole of the O-terminated plane, oxygen vacancies are created in the O-terminated surface. The resulting half-vacant oxygen-terminated surface is very unstable (Table 8), especially compared to the single iron-terminated {0001} plane, and the oxygen vacancies are very attractive sites for the dissociative adsorption of water, where the hydroxy groups fill the vacancies and the protons attach to the remaining surface oxygen ions leading to a smooth plane of hydroxy groups as shown in Fig. 4(a). As we can see from Table 9, adsorption of molecular water at the iron-terminated surface is energetically favourable and so is hydration of dissociated water when one water molecule per surface Fe(III) ion is adsorbed leading to the structure shown in Fig. 4(b). However, when three dissociated water molecules are adsorbed per surface Fe(III) ion, i.e. three added hydroxy groups complete the coordination of the surface Fe(III) ions and all surface oxygen ions in the layer below have been protonated, the hydration energy becomes positive ($+6.1$ kJ mol^{-1}) and the surface is destabilized ($\gamma = 1.92$ J m^{-2}) with respect to the dehydrated surface. In fact, this structure is similar to the hydroxylated oxygen-terminated surface, but with the topmost sub-surface Fe(III) ions replaced by three protons each attached to the oxygen ions in the second oxygen layer. It is therefore not surprising that this structure, which is essentially an iron-defective plane, is less stable than either the dehydrated or partially hydrated iron-terminated

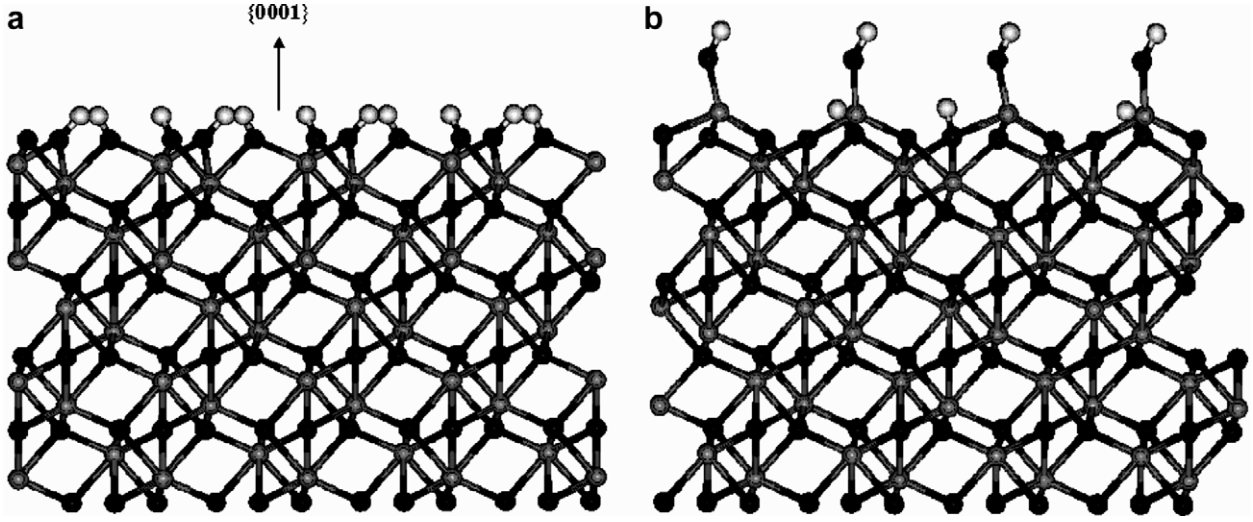

Fig. 4. Geometry-optimized hematite {0001} surfaces, showing (a) the fully hydroxylated oxygen-terminated surface with surface hydroxy groups located in its former oxygen vacancies, and (b) the partially hydroxylated iron-terminated surface (Fe, grey; O, black; H, white; distances shown in Å).

surface. When hydrated, the oxygen-terminated surface has thus become much more stable than the iron-terminated surface and we would therefore expect the oxygen-terminated surface to occur under aqueous conditions, although, if the crystal were cleaved under ultra-high vacuum conditions the (dehydrated) iron-terminated {0001} surface should occur, in agreement with the molecular beam epitaxy study by Chambers and Yi (1999), who found only the Fe-terminated surface, even under highly oxidizing conditions. This iron-terminated plane shows strong relaxations of the surface layers and interlayer spacings, which in Fig. 5 are compared with experimentally observed interlayer spacings (Thevuthasan et al., 1999). The discrepancy between experiment and calculation in the relaxation of the topmost Fe layer may be due to overestimation of the relaxation in the computational model or to residual water in the experimental set up, which would lessen the relaxation of the surface Fe(III) ions into the bulk material.

Interlayer spacings / Å

Surface Layer		
Simulation		**Experiment**[a]
	Fe	
0.21		**0.50**
	Ox	
0.90		**1.00**
	Fe	
0.42		**0.55**
	Fe	
0.97		**1.24**
	Ox	
0.87		**0.84**
	Fe	
0.61		**0.61**
	Fe	

[a] Thevuthasan et al. (1999)

Fig. 5. Comparison of calculated and experimental interlayer spacings of the Fe-terminated hematite {0001} surface.

Recent experimental studies of the interaction of water with the hematite {0001} and $\{01\bar{1}2\}$ surfaces include the synchrotron X-ray photoemission studies by Liu et al. (1998), TPD measurements by Henderson et al. (1998), scanning tunneling microscopy and resonant tunneling calculations by Eggleston et al. (2003) and crystal truncation rod studies by Trainor et al. (2004). Liu et al.'s study of single crystal thin films of hematite grown on α-alumina showed that hydroxylation of the (0001) surface takes place above a threshold water pressure of 1.33×10^{-4} mbar, below which pressure a limited but persistent amount of surface hydroxylation is observed, which they attribute to surface defects. Eggleston et al. (2003) have identified that under aqueous conditions both Fe- and O-terminations of the {0001} surface co-exist in distinct domains. Although our calculations suggest that the oxygen-terminated surface should be more stable than the iron-terminated plane, in agreement with Trainor et al. (2004), Eggleston et al. have pointed out that the two planes are inter-convertible through the dissolution of surface species and hence there is a mechanism for the formation of both surfaces under aqueous conditions. Furthermore, it is likely that there is an activation energy to the dissociation of molecular water at the surface, and as our calculations have shown that the Fe-terminated surface is more stable than the O-termination when hydrated by molecular water, both surface terminations could thus have a finite lifespan.

Computationally, the structure of the {0001} and $\{01\bar{1}2\}$ surfaces of hematite and their interaction with water have been studied by Wasserman et al. (1997), Parker and co-workers (Parker et al., 1999; Cooke et al., 2004) and Lado-Touriño and Tsobnang (2000); using similar computational methods and obtaining similar results to our own, although the absolute surface energies vary somewhat

with the variation in potential model or computational techniques used. For example, the surface energy of the dehydrated iron-terminated {0001} surface is calculated to range from 1.52 J m^{-2} (Wang et al., 1998), using density functional theory calculations, to 1.53 J m^{-2} (Mackrodt et al., 1987), 1.65 J m^{-2} (Wasserman et al., 1997), 1.78 J m^{-2} (this work), 2.24 J m^{-2} (Cooke et al., 2004) and even 22.34 J m^{-2} (Lado-Touriño and Tsobnang, 2000), depending on the potential model used, although the last value appears rather large compared to all other computed values. Unfortunately, to the authors' knowledge no reliable experimental values are available.

The $\{01\bar{1}2\}$ surface can have a number of non-dipolar terminations, all of which we have considered. However, one termination is consistently calculated to be more stable, whether dehydrated or hydrated by associatively or dissociatively adsorbed water molecules and this surface is therefore listed in Tables 8 and 9 and shown in Fig. 6 with an associatively adsorbed water layer, where the water molecules are coordinated by their oxygen ions to surface Fe(III) ions at 2.08 Å. The water molecules form a network of hydrogen-bonded interactions, both intermolecularly and to the surface with O–H distances ranging from 1.74 to 2.08 Å. The reason for the stability of this particular surface termination is due to the layered structure of the $\{01\bar{1}2\}$ surface, with an interlayer distance of approximately 1.5 Å between the topmost oxygen ions of one layer and the bottommost oxygen ions of the next layer (2.1 Å between top and bottom Fe(III) ions). We can clearly see that the plane shown in Fig. 6 is cleaved between these layers and terminated by a smooth layer of both Fe(III) and oxygen ions.

In addition to the above (1×1) surface, Henderson et al. (1998) have used low energy electron diffraction (LEED) under ultra-high vacuum (UHV) conditions to study the $\{01\bar{1}2\}$ surface and they observed an alternative (1×2) surface termination with a greater surface concentration of cation sites than the (1×1) surface. From our calculations, we would suggest that this observed plane is the next most stable termination ($\gamma = 2.36$ J m^{-2}), which has only half a layer of oxygen ions in the topmost layer, with a full layer of Fe ions underneath, which are hence exposed at the surface. This surface still adsorbs water dissociatively, again in agreement with Henderson et al. (1998).

In addition to the {0001} and $\{01\bar{1}2\}$ surfaces, the $\{10\bar{1}1\}$ surface is another important surface, observed in both cleavage and twinning (Deer et al., 1992) and, as can be seen from the surface energies in Table 8, quite a few other surfaces have similar stabilities and thus merit investigation. When dehydrated, the $\{10\bar{1}1\}$ surface is one of the least stable of the surfaces considered here ($\gamma = 2.34$ J m^{-2}). However, it is stabilized considerably through hydration, first by associatively adsorbed water molecules and then further upon dissociation of the water, to one of the most stable surfaces, in agreement with its experimental significance. Fig. 7 shows the dehydrated and hydroxylated $\{10\bar{1}1\}$ surfaces. The instability of the dehydrated surface is due to the low-coordination of the surface ions: four-coordinated Fe(III) ions, instead of their bulk coordination of six, and either two- or three-coordinated oxygen ions, instead of their bulk coordination of four. Upon dissociative adsorption of water at the surface, all surface Fe(III) ions have increased their coordination to the bulk value of six, whereas the surface oxygen ions have become either three- or four-coordinated, and the surface as a result has become more bulk-like leading to its increased stability. The surface hydroxy groups form an extended network of hydrogen-bonded interactions with O–H distances ranging from 1.95 to 2.65 Å.

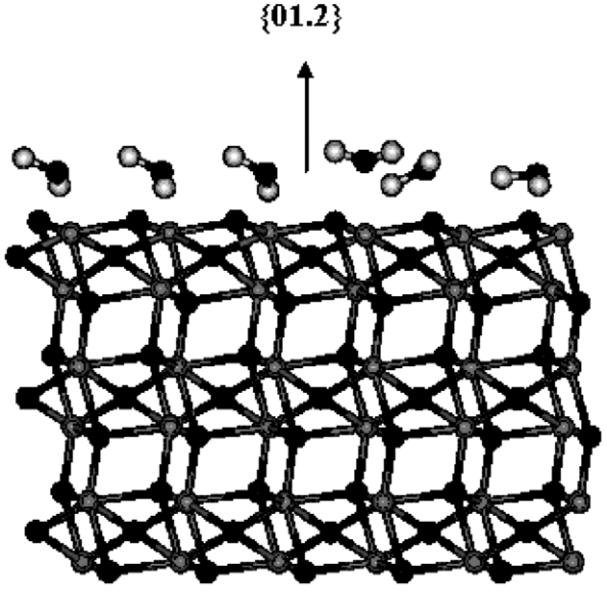

Fig. 6. Geometry-optimized hematite $\{01\bar{1}2\}$ surface with associatively adsorbed water molecules, showing the layered structure (Fe, grey; O, black; H, white; distances shown in Å).

3.4. Morphologies

From the surface energies of the hydrated and hydroxylated hematite, goethite and $Fe(OH)_2$ surfaces, we have calculated the equilibrium morphologies for these minerals in an aqueous environment, where the surfaces for which the energy of dissociative adsorption was equal or less than that of associative adsorption were deemed not to become hydroxylated. However, apart from the $Fe(OH)_2$ surfaces, where dissociative adsorption cannot occur, and the goethite {010} surface, dissociative adsorption of water is energetically more favourable than molecular adsorption of water in all cases and we have therefore used the surface energies of these hydroxylated surfaces to calculate the morphologies. Fig. 8(a) shows an experimentally determined morphology for hematite, showing the dominance of the {0001} and $\{10\bar{1}1\}$ planes (Goldschmidt, 1913), although a considerable number of hematite morphologies with additional surfaces have been found, depending on the growth conditions (Goldschmidt, 1913; Stipp et al., 2002; Glotch et al., 2004). The calculated equilibrium morphologies for the three minerals are shown in Figs. 8(b)–(d) and we see that the calculated morphology for hematite is in good agreement with the experimentally found morphology, only showing some extra $\{01\bar{1}1\}$ surface at

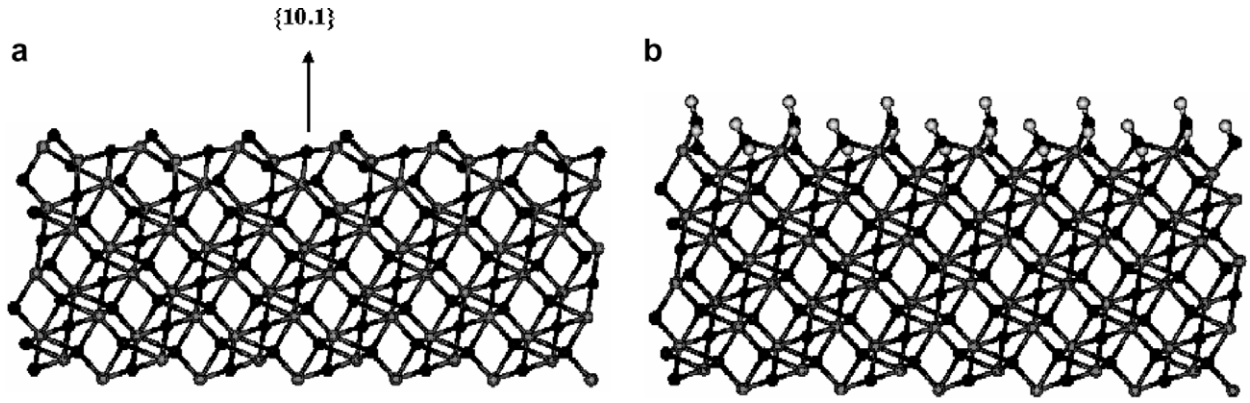

Fig. 7. Geometry-optimised hematite $\{10\bar{1}1\}$ surface, (a) before and (b) after dissociative adsorption of water, showing bulk-like termination of the hydroxylated surface (Fe, grey; O, black; H, white; distances shown in Å).

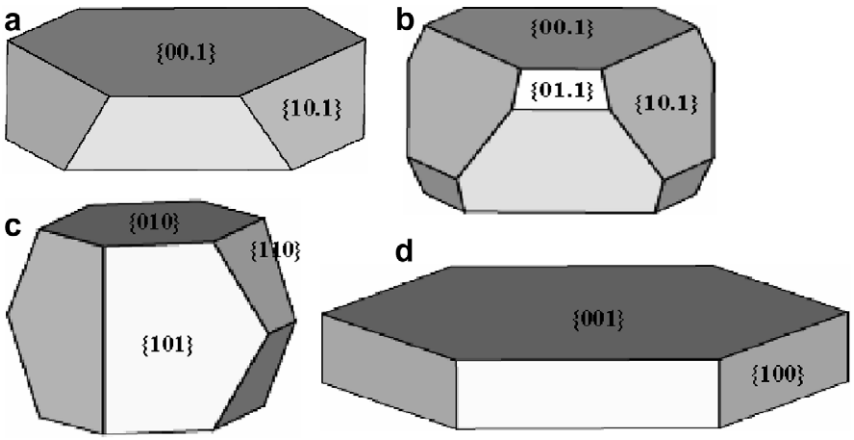

Fig. 8. (a) Experimental and (b) calculated morphologies of hematite, and calculated morphologies of (c) goethite and (d) iron hydroxide.

the expense of the $\{10\bar{1}1\}$ plane. Goethite has been found in a bewildering number of morphologies (e.g. Deer et al., 1992), with the one common denominator that the {010} surface, which is the perfect cleavage plane, is almost always present and often the {110} and {101} surfaces as well, all of which are expressed in the calculated morphology. The morphology of $Fe(OH)_2$, for which an experimental morphology is not known, resembles that of the hematite crystal, expressing only the {100} and, as expected, the {001} surfaces.

3.5. Dehydration partial pressures and temperatures

Water on Mars is found both as widespread sub-surface ice sheets near the poles and as mineral-bound water near the equator (McSween, 2006). Enrichment of heavy isotopes of hydrogen and oxygen measured in Martian meteorites show that water is cycled from the crust to the atmosphere and back again, due to cyclic changes in the Martian climate caused by oscillations in the axial tilt, eccentricity and timing of the closest approach to the Sun (Christensen, 2006). Because of the interest in water adsorption at iron-containing minerals on Mars and especially whether the planet may have had a warmer, wetter atmosphere in the past which would be inducive to the development of life, we wished to investigate the partial pressures and temperatures at which water would be retained at the mineral surfaces. We have only considered goethite and hematite for two reasons; first, these two stable minerals have been identified to occur on Mars, and second, water at the $Fe(OH)_2$ surfaces is only adsorbed associatively, a weak interaction that would not retain water at low partial pressures or higher temperatures (Fubini et al., 1989). We therefore have calculated the pressure/temperature relationships for dissociative adsorption of water at the hematite and goethite surfaces.

In order to calculate the partial pressures of gaseous water required for appreciative adsorption of water at the iron (hydr)oxide surfaces at higher temperatures, we need to consider the process of adsorption of a water molecule at the mineral surface, according to the following Eq. (7):

$$\text{Surface} + H_2O_{(g)} \overset{K}{\leftrightarrow} \text{Surface} \cdot (H_2O) \tag{7}$$

where K is the equilibrium constant for the above reaction, *Surface* is the mineral surface before water adsorption and Surface·(H_2O) is the system after adsorption. The equilibrium constant K is then calculated as shown in Eq. (8), from the Gibbs free energy G of adsorption, where $a_{(s)}$ and $a_{(g)}$ are the activities of the water molecule adsorbed at the solid

surface or in its gaseous state, respectively. Following the simple Langmuir model, we can write the activities of the partially hydrated surface as $x/(1-x)$, where x is the fraction of surface sites occupied by water, $p_{H_2O_{(g)}}$ is the partial pressure of gaseous water, which is the quantity we seek to calculate, R is the gas constant and T is the temperature of interest.

$$K = \frac{a_{(s)}}{a_{(g)}a_{surface}} = \frac{x}{(1-x)p_{H_2O_{(g)}}} = e^{-\Delta G^0/RT} \quad (8)$$

Following de Leeuw et al. (2006), in these calculations where we consider water adsorption at low partial pressures, adsorption of a complete monolayer is unrealistic and we have therefore used the hydration energy of isolated (gaseous) water molecules at the energetically preferred adsorption site, where we can calculate the fractional occupancy x from our knowledge of the maximum number of water molecules in the full monolayer.

Table 10
Entropies of gaseous water

Temperature (K)	S (JK^{-1} mol^{-1}) at 1 bar	$T\Delta S$ (kJ mol^{-1}) (Eq. 1)
273.15	0	0
298	188.832	−56.3
400	198.791	−79.5
500	206.542	−103.3
600	213.067	−127.8
700	218.762	−153.1
800	223.858	−179.1
900	228.501	−205.7
1000	232.792	−232.8
1100	236.797	−260.5
1200	240.565	−288.7
1300	244.129	−317.4
1400	247.516	−346.5
1500	250.745	−376.1

$$\Delta G = \Delta H - T\Delta S \quad (9)$$

The change in the standard Gibbs free energies for adsorption of water at the various iron (hydr)oxide surfaces according to Eq. (7) were calculated from the enthalpies and entropies at the required temperatures (Eq. (9)), where ΔH is the enthalpy of the adsorption process per water molecule, T is the temperature of interest and ΔS is the change in entropy. The enthalpies for the hydration of the hematite and goethite mineral surfaces are obtained directly from our simulations, but in addition we require the entropies of gaseous water. We have used experimental entropies for the gaseous water molecule at various temperatures, as listed in Table 10 (Lide, 2000).

In order to calculate the Gibbs free energies of the adsorption processes, we now make two assumptions. First, if we assume that the entropies of the iron (hydr)oxide minerals remain largely unaffected by the surface adsorption of the water molecule, then we need only take into account the change in entropy due to the loss of the free water molecule from the gaseous state onto the surface adsorption sites. The assumption, that the entropy of the mineral surface remains largely unchanged when a small molecule is adsorbed at the surface, has already been used in entropy calculations of the ad- and desorption of $Si(OH)_4$ species from quartz surfaces, where the calculated trends were shown to be in good agreement with experiment (Du and de Leeuw, 2006). Second, we assume that the enthalpies of the adsorption processes, which are calculated without taking into account the temperature of the system, will not be affected significantly by temperature (other than the entropy change in the water molecule). As the hydration enthalpies are lattice energy differences rather than absolute values, we consider that this is a reasonable approximation. Taking

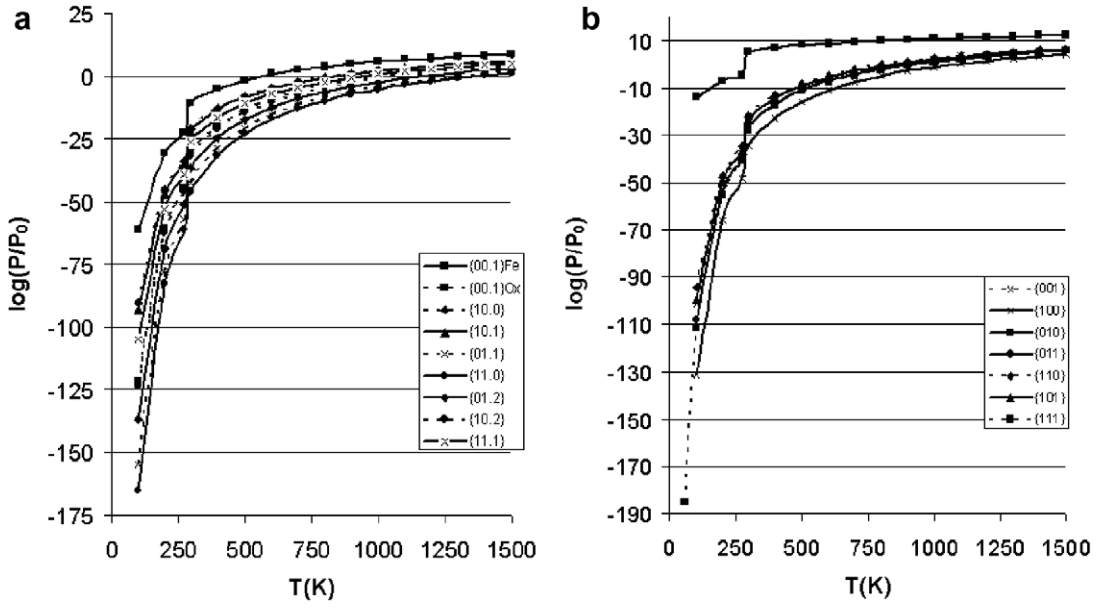

Fig. 9. Calculated pressure/temperature dependence of dissociative water adsorption at (a) hematite and (b) goethite surfaces.

into account these two approximations, we then can calculate the Gibbs free energies for the adsorption processes, according to Eq. (9). Using the calculated Gibbs free energies at each temperature and for each mineral surface, we can now calculate from Eq. (8) the partial pressures of water at which this adsorption would occur.

The partial pressure versus temperature plots for the dissociative adsorption of water at hematite and goethite surfaces are shown in Fig. 9. The two graphs show that the curves for the hematite surfaces are more spread out than those for the goethite surfaces. Some of the very reactive hematite surfaces, for example the $\{11\bar{2}0\}$ and $\{01\bar{1}1\}$ surfaces, adsorb water at relative high temperatures and/or low partial water pressures. As large hematite deposits are present on Mars, from our calculations it would appear that these mineral deposits could be significant contributors in the retention of water on this planet from earlier, wetter periods in the planet's climate, which could be cycled back into its atmosphere when the temperature is raised as the planet's orbit brings it closer to the Sun.

4. CONCLUSIONS

We have derived an interatomic potential model for iron oxyhydroxides in aqueous environment, which is transferable to a large number, if not all, iron oxide phases. We have applied this new interatomic potential in an extensive computer modelling study of the hydration of a range of surfaces of three representative iron-bearing minerals by associative and dissociative adsorption of water, which has shown the following general trends:

- The major interaction between the adsorbing water molecules and the surface is through interaction of their oxygen ions with surface iron ions, followed by hydrogen-bonding to surface oxygen ions. Hydrogen-bonded networks of hydroxy groups and water molecules stabilise the hydrated structures, but the hydration energy also depends on the initial and final structures of the mineral surface. Dissociative adsorption does not occur when the surface oxygen ion is already in its full bulk-coordination.
- The calculated hematite morphology is in fair agreement with experimental morphologies and the calculated goethite morphology expresses the main surfaces as seen experimentally. An iron hydroxide morphology is not known, but based on the agreement of the morphologies of hematite and goethite with experiment, the calculated morphology of $Fe(OH)_2$ seems reasonable in view of the structure of the surfaces investigated.
- The calculated partial pressures required for water adsorption from the gas phase to occur at hematite and goethite surfaces at a range of temperatures show that these minerals may be instrumental in retaining water for further recycling into the atmosphere of Mars. Note that the values shown in this work are in fact lower limits for the temperatures and upper limits for the partial pressures, as reactive defects at the surfaces, including Fe and O vacancies and low-coordinated surfaces sites due to steps and corners, will lead to larger hydration energies and hence lower partial pressures required to retain water at higher temperatures.

Future work will include the consideration of a range of surface defects in hydration calculations of these and other iron-bearing minerals, such as Fe_3O_4, lepidocrocite and green rust. In addition, we will also investigate hydration behaviour from the gas phase using Molecular Dynamics simulations to include temperature and pressure into the simulations in order to mimic the Mars atmosphere more directly. Finally, we will extend our present study of the adsorption of water at the iron (hydr)oxide surfaces to include the immobilisation of toxic arsenic species at the mineral surfaces as well as the adsorption of organic contaminants (de Leeuw and Cooper, 2004).

ACKNOWLEDGMENTS

We thank Professor Susan Stipp, Dr. Marilena Stimpfl, Professor Mike Drake and Professor Richard Catlow for useful discussions, and anonymous reviewers for their comments. N.H.d.L. also thanks the Engineering and Physical Sciences Research Council, UK for an Advanced Research Fellowship and for Grant No. GR/S44662/01. We also acknowledge the use of the EPSRC's Chemical Database Service at Daresbury.

REFERENCES

Allan N. L., Barrera G. D., Purton J. A., Sims C. E., and Taylor M. B. (2000) Ionic solids at elevated temperatures and/or high pressures: lattice dynamics, molecular dynamics, Monte Carlo and ab initio studies. *Phys. Chem. Chem. Phys.* **2**, 1099–1111.

Allen C. C., Probst L. W., Flood B. E., Longazo T. G., Schelble R. T., and Westall F. (2004) Meridiani Planum hematite deposit and the search for evidence of life on Mars—iron mineralization of microorganisms in rock varnish. *Icarus* **171**, 20–30.

Archuleta C. M., DeMott P. J., and Kreidenweis S. M. (2005) Ice nucleation by surrogates for atmospheric mineral dust and mineral dust/sulfate particles at cirrus temperatures. *Atmos. Chem. Phys.* **5**, 2617–2634.

Baltrusaitis J., and Grassian V. H. (2005) Surface reactions of carbon dioxide at the adsorbed water-iron oxide interface. *J. Phys. Chem. B* **109**, 12227–12230.

Baram P. S., and Parker S. C. (1996) Atomistic simulation of hydroxide ions in inorganic solids. *Philos. Mag. B* **73**, 49–58.

Baumgärtel H., Grünbein W., and Hensel F. (1999) Global aspects of atmospheric chemistry. In *Topics in Physical Chemistry: 6*. Steinkopff, Darmstadt.

Bell J. F., McSween H. Y., Crisp J. A., Morris R. V., Murchie S. T., Bridges N. T., Johnson J. R., Britt D. T., Golombek M. P., Moore H. J., Ghosh A., Bishop J. L., Anderson R. C., Bruckner J., Economou T., Greenwood J. P., Gunnlaugsson H. M., Hargraves R. M., Hviid S., Knudsen J. M., Madsen M. B., Reid R., Rieder R., and Soderblom L. (2000) Mineralogic and compositional properties of Martian soil and dust: results from Mars Pathfinder. *J. Geophys. Res.—Planet* **105**, 1721–1755.

Born M., and Huang K. (1954) *Dynamical Theory of Crystal Lattices*. Oxford University Press, Oxford.

Catlow C. R. A., James R., Mackrodt W. C., and Stewart R. F. (1982) Defect energies in alpha-Al_2O_3 and rutile TiO_2. *Phys. Rev. B: Condens. Matter* **25**, 1006–1026.

Cerny R., Valvoda V., and Chladek M. (1995) Empirical texture corrections for asymmetric diffraction and inclined textures. *J. Appl. Crystallogr.* **28**, 247–253.

Chambers S. A., and Yi S. I. (1999) Fe termination for α-Fe_2O_3 (0001) as grown by oxygen-plasma-assisted molecular beam epitaxy. *Surf. Sci.* **439**, L785–L791.

Chevrier V., Rochette P., Mathe P. E., and Grauby O. (2004) Weathering of iron-rich phases in simulated Martian atmospheres. *Geology* **32**, 1033–1036.

Ching W. Y., and Xu Y-N. (1994) First-principles calculation of electronic, optical, and structural properties of alpha-Al_2O_3. *J. Am. Ceram. Soc.* **77**, 404–411.

Christensen A. N., Hansen P., and Lehmann M. S. (1976) Isotope effects in bonds of beta-CrOOH and beta-CrOOD. *J. Solid State Chem.* **19**, 299–304.

Christensen P. R. (2006) Water at the poles and in permafrost regions of Mars. *Elements* **2**, 151–155.

Christensen P. R., Bandfield J. L., Clark R. N., Edgett K. S., Hamilton V. E., Hoefen T., Kieffer H. H., Kuzmin R. O., Lane M. D., Malin M. C., Morris R. V., Pearl J. C., Pearson R., Roush T. L., Ruff S. W., and Smith M. D. (2000) Detection of crystalline hematite mineralization on Mars by the thermal emission spectrometer: evidence for near-surface water. *J. Geophys. Res.—Planet* **105**, 9623–9642.

Chung K. W., Kim K. B., Han S-H., and Lee H. (2005) Novel synthesis of nanosized cellular iron oxide/oxyhydroxide thin films—I. Electrochemical synthesis of green rust thin films and their chemical oxidation. *J. Electrochem. Soc.* **152**, C560–C565.

Cooke D. J., Redfern S. E., and Parker S. C. (2004) Atomistic simulation of the structure and segregation to the (0001) and (01–12) surfaces of Fe_2O_3. *Phys. Chem. Miner.* **31**, 507–517.

Cooper T. G., and de Leeuw N. H. (2003) A combined ab initio and atomistic simulation study of the surface and interfacial structures and energies of hydrated scheelite: introducing a $CaWO_4$ potential model. *Surf. Sci.* **531**, 159–176.

Cooper T. G., and de Leeuw N. H. (2006) A computer modelling study of the incorporation of K^+, Ca^{2+} and Mg^{2+} impurities in two Na_2SO_4 polymorphs: Introducing a Na_2SO_4 potential model. *J. Cryst. Growth* **294**, 137–149.

Coustet V., and Jupille J. (1994) High-resolution electron-energy-loss spectroscopy of isolated hydroxyl-groups on alpha-Al_2O_3 (0001). *Surf. Sci.* **309**, 1161–1165.

Cox D. E., Takei W. J., Miller C., and Shirane G. (1962) Magnetic and neutron diffraction study of Fe_2O_3—V_2O_3 system. *J. Phys. Chem. Solids* **23**, 863.

de Leeuw N. H., and Cooper T. G. (2003) A computational study of the surface structure and reactivity of calcium fluoride. *J. Mater. Chem.* **13**, 93–101.

de Leeuw N. H., and Cooper T. G. (2004) A computer modeling study of the inhibiting effect of organic adsorbates on calcite crystal growth. *Cryst. Growth Des.* **4**, 123–133.

de Leeuw N. H., Du Z. M., Li J., Yip S., and Zhu T. (2003) Computer modelling of the effect of hydration on the stability of a silica nanotube. *Nano Lett.* **3**, 1347–1352.

de Leeuw N. H., Higgins F. M., and Parker S. C. (1999) Modeling the surface structure and stability of alpha-quartz. *J. Phys. Chem. B* **103**, 1270–1277.

de Leeuw N. H., and Parker S. C. (1997) Atomistic simulation of the effect of molecular adsorption of water on the surface structure and energies of calcite surfaces. *J. Chem. Soc. Faraday Trans.* **93**, 467–475.

de Leeuw N. H., and Parker S. C. (1998a) Molecular-dynamics simulations of MgO surfaces in liquid water using a shell-model potential for water. *Phys. Rev. B* **58**, 13901–13908.

de Leeuw N. H., and Parker S. C. (1998b) Surface structure and morphology of calcium carbonate polymorphs calcite, aragonite and vaterite: An atomistic approach. *J. Phys. Chem. B* **102**, 2914–2922.

de Leeuw N. H., and Parker S. C. (1999) Effect of chemisorption and physisorption of water on the surface structure and stability of alpha-alumina. *J. Am. Ceram. Soc.* **82**, 3209–3216.

de Leeuw N. H., Parker S. C., Catlow C. R. A., and Price G. D. (2000) Modelling the effect of water on the surface structure and stability of forsterite. *Phys. Chem. Miner.* **27**, 332–341.

de Leeuw N. H., Watson G. W., and Parker S. C. (1996) Atomistic simulation of the adsorption of water on three-, four- and five-coordinated surface sites of magnesium oxide. *J. Chem. Soc. Faraday Trans.* **92**, 2081.

de Leeuw, N. H., Stimpfl, M., Catlow, C. R. A., Drake, M. J., Deymier, P. A., and Walker, A. W. (2006) Can the water pressure in the accretion disk sustain water adsorption on olivine? In Sixty-Ninth Annual Meteoritical Soc Meeting, Contribution 5015.

Deer W. A., Howie R. A., and Zussman J. (1992) An Introduction to the Rock-forming Minerals. Longman Group, Harlow, UK.

Dick, Jr., B. G., and Overhauser A. W. (1958) Theory of the dielectric constants of alkali halide crystals. *Phys. Rev.* **112**, 90–103.

Du Z., and de Leeuw N. H. (2006) Molecular dynamics simulations of hydration, dissolution and nucleation processes at the α-quartz (0001) surface in liquid water. *Dalton Trans.* **22**, 2623–2634.

Du Z. M., and de Leeuw N. H. (2004) A combined density functional theory and interatomic potential-based simulation study of the hydration of nano-particulate silicate. *Surf. Sci.* **2–3**, 193–210.

Edwards H. G. M., Wynn-Williams D. D., and Villar S. E. J. (2004) Biological modification of haematite in Antarctic cryptoendolithic communities. *J. Raman Spectrosc.* **35**, 470–474.

Eggleston C. M., Stack A. G., Rosso K. M., Higgins S. R., Bice A. W., Boese S. W., Pribyl R. D., and Nichols J. J. (2003) The structure of hematite (α-Fe_2O_3) (001) surfaces in aqueous media: scanning tunneling microscopy and resonant tunneling calculations of coexisting O and Fe terminations. *Geochim. Cosmochim. Acta* **67**, 985–1000.

Fenter P., Geissbuhler P., DiMasi E., Srajer G., Sorensen L. B., and Sturchio N. C. (2000) Surface speciation of calcite observed in situ by high-resolution X-ray reflectivity. *Geochim. Cosmochim. Acta* **64**, 1221–1228.

Fjellvag H., Gronvold F., and Stolen S. (1996) On the crystallographic and magnetic structures of nearly stoichiometric iron monoxide. *J. Solid State Chem.* **124**, 52–57.

Fletcher D. A., McMeeking R. F., and Parkin D. (1996) The United Kingdom chemical database service. *J. Chem. Inf. Comput. Sci.* **36**, 746–749.

Fubini B., Bolis V., Bailes M., and Stone F. (1989) The reactivity of oxides with water-vapor. *Solid State Ionics*(32/33), 258–272.

Gibbs J. W. (1928) Collected Works. Longman, New York.

Gillet E., and Ealet B. (1992) Characterization of sapphire surfaces by electron energy-loss spectroscopy. *Surf. Sci.* **273**, 236–427.

Glotch T. D., Morris R. V., Christensen P. R., and Sharp T. G. (2004) Effect of precursor mineralogy on the thermal infrared emission spectra of hematite: application to Martian hematite mineralization. *J. Geophys. Res.* **109**, E07003.

Godin T. J., and LaFemina J. P. (1994) Atomic and electronic structure of the corundum (alpha-alumina) (0001) surface. *Phys. Rev. B: Condens. Matter* **49**, 7691–7696.

Goldschmidt V. M. (1913). *Der Atlas der Krystallformen*, 319.

Guo J., Ellis D. E., and Lam D. J. (1992) Electronic-structure and energetics of sapphire (0001) and (1102) surfaces. *Phys. Rev. B* **45**, 13647–13656.

Hazemann J. L., Manceau A., Sainctavit P., and Malgrange C. (1992) Structure of the alpha-$Fe_xAl_{1-x}OOH$ solid solution 1. Evidence by polarisec EXAFS for an epitaxial-growth of hematite-like clusters in Fe-diaspore. *Phys. Chem. Miner.* **19**, 25–38.

Henderson M. A., Joyce S. A., and Rustad J. R. (1998) Interaction of water with the (1x1) aned (2x1) surfaces of α-Fe_2O_3 (012). *Surf. Sci.* **417**, 66–81.

Hendy S., Walker B., Laycock N., and Ryan M. (2003) Ab initio studies of the passive film formed on iron. *Phys. Rev. B* **67**, 085407.

Hendy S. C., Laycock N. J., and Ryan M. P. (2005) Atomistic modeling of cation transport in the passive film on iron and implications for models of growth kinetics. *J. Electrochem. Soc.* **152**, B271–B276.

Iizumi M., Koetzle T. F., Shirane G., Chikazumi S., Matsui M., and Todo S. (1982) Structure of magnetite (Fe_3O_4) below the Verwey transition-temperature. *Acta Crystallogr. B* **38**, 2121–2133.

Jia C-J., Sun L-D., Yan Z-G., You L-P., Luo F., Han X-D., Pang Y-C., Zhang Z., and Yan C-H. (2005) Iron oxide nanotubes—Single-crystal iron oxide nanotubes. *Angew. Chem. Int. Ed.* **44**, 4328–4333.

Jolivet J. P., Chanéac C., and Tronc E. (2004) Iron oxide chemistry from molecular clusters to extended solid networks. *Chem. Commun.*, 481–487.

Jones F., Rohl A. L., Farrow J. B., and Van Bronswijk W. (2000) Molecular modeling of water adsorption on hematite. *Phys. Chem. Chem. Phys.* **2**, 3209–3216.

Jones N. O., Reddy B. V., Rasouli F., and Khanna S. N. (2005) Structural growth in iron oxide clusters: Rings, towers, and hollow drums. *Phys. Rev. B* **72**, 165411.

Kerisit S., and Parker S. C. (2004a) Free energy of adsorption of water and calcium on the {10–14} calcite surface. *Chem. Commun.*, 52–53.

Kerisit S., and Parker S. C. (2004b) Free energy of adsorption of water and metal ions on the {1014} calcite surface. *J. Am. Chem. Soc.* **126**, 10152–10161.

Kerisit S., Cooke D. J., Marmier A., and Parker S. C. (2005) Atomistic simulation of charged iron oxyhydroxide surfaces in contact with aqueous solution. *Chem. Commun.*, 3027–3029.

Ketteler G., Weiss W., Ranke W., and Schlögl R. (2001) Bulk and surface phases of iron oxides in an oxygen and water atmosphere at low pressures. *Phys. Chem. Chem. Phys.* **3**, 1114–1122.

Kim D-Y., Wiederhorn S. M., Hockey B. J., Handwerker C. A., and Blendell J. E. (1994) Stability and surface energies of wetted grain-boundaries in aluminum-oxide. *J. Am. Ceram. Soc.* **77**, 444–453.

Lado-Touriño I., and Tsobnang F. (2000) Using computational approaches to model hematite surfaces. *Comp. Mater. Sci.* **17**, 243–248.

Lane M. D., Morris R. V., Mertzman S. A., and Christensen P. R. (2002) Evidence for platy hematite grains in Sinus Meridiani, Mars. *J. Geophys. Res.—Planet* **107**, 5126.

Lei Y., Cant N. W., and Trimm D. L. (2005) Activity patterns for the water gas shift reaction over supported precious metal catalysts. *Catal. Lett.* **103**, 133–136.

Leist U., Ranke W., and Al-Shamery K. (2003) Water adsorption and growth of ice on epitaxial Fe_3O_4(111), FeO(111) and Fe_2O_3(biphase). *Phys. Chem. Chem. Phys.* **5**, 2435–2441.

Lewis G. V., and Catlow C. R. A. (1985) Potential models for ionic oxides. *J. Phys. C: Solid State Phys.* **18**, 1149–1161.

Liang Y., Lea A. S., Baer D. R., and Engelhard M. H. (1996) Structure of the cleaved $CaCO_3$ (10(1)over-bar4) surface in an aqueous environment. *Surf. Sci.* **351**, 172–182.

Lide D. R. (2000) CRC Handbook of Chemistry and Physics. CRC, Boca Raton, USA.

Liu P., Kendelewicz T., Brown, Jr., G. E., Nelson E. J., and Chambers S. A. (1998) Reaction of water vapor with α-Al_2O_3 (0001) and α-Fe_2O_3 (0001) surfaces: synchrotron X-ray photoemission studies and thermodynamic calculations. *Surf. Sci.* **417**, 53–65.

Loffler L., and Mader W. (2006) Anisotropic X-ray peak broadening and twin formation in hematite derived from natural and synthetic goethite. *J. Eur. Ceram. Soc.* **26**, 131–139.

Lutz H. D., Möller H., and Schmidt M. (1994) Lattice vibration spectra. Part LXXXII. Brucite-type hydroxides $M(OH)_2$ (M=Ca, Mn, Co, Fe, Cd)—IR and Raman spectra, neutron diffraction of $Fe(OH)_2$. *J. Mol. Struct.* **328**, 121–132.

Mackrodt W. C. (1992). *Philos. Trans. R. Soc. London A* **341**, 301.

Mackrodt W. C., Davey R. J., Black S. N., and Docherty R. (1987) The morphology of alpha-Al_2O_3 and alpha-Fe_2O_3—the importance of surface relaxation. *J. Cryst. Growth* **80**, 441–446.

Majzlan J., Grevel K. D., and Navrotsky A. (2003) Thermodynamics of Fe oxides: Part II. Enthalpies of formation and relative stability of goethite (alpha-FeOOH), lepidocrocite (gamma-FeOOH), and maghemite (gamma-Fe_2O_3). *Am. Miner.* **88**, 855–859.

Manassidis I., and Gillan M. J. (1994) Structure and energetics of alumina surfaces calculated from first principles. *J. Am. Ceram. Soc.* **77**, 335–338.

Mann S., Webb J., and Williams R. J. P. (1989) Biomineralization in Chemical and Biological Perspectives. VCH, New York.

McSween, Jr., H. Y. (2006) Water on Mars. *Elements* **2**, 135–137.

Meng X., Korfiatis G. P., Bang S. B., and Bang K. W. (2002) Combined effects of anions on arsenic removal by iron hydroxides. *Toxicol. Lett.* **133**, 103–111.

Meskhidze N., Chameides W. L., Nenes A., and Chen G. (2003) Iron mobilization in mineral dust: Can anthropogenic SO_2 emissions affect ocean productivity? *Geophys. Res. Lett.* **30**, 2085.

Mkhonto D., and de Leeuw N. H. (2002) A computer modelling study of the effect of water on the surface structure and morphology of fluorapatite: introducing a $Ca_{10}(PO_4)_6F_2$ potential model. *J. Mater. Chem.* **12**, 2633–2642.

Morris R. V., Golden D. C., Bell J. F., Shelfer T. D., Scheinost A. W., Hinman N. W., Furniss G., Mertzman S. A., Bishop J. L., Ming D. W., Allen C. C., and Britt D. T. (2000) Mineralogy, composition, and alteration of Mars Pathfinder rocks and soils: Evidence from multispectral, elemental and magnetic data on terrestrial analogue, SNC meteorite and Pathfinder samples. *J. Geophys. Res.—Planet* **105**, 1757–1817.

Muhler M., Schütze J., Wesemann M., Rayment T., Dent A., Schlögl R., and Ertl G. (1990) The nature of the iron oxide-based catalyst for dehydrogenation of ethylbenzene to styrene 1. Solid-state chemistry and bulk characterization. *J. Catal.* **126**, 339–360.

Mulheran P. A. (1993) Structural calculations of oxide surfaces at finite-temperature. *Philos. Mag. A* **68**, 799–808.

Natta G. (1928) Constitution of hydroxides and hydrates. *Gazz. Chimica Italiana* **58**, 344–358.

Newsom H. E., Barber C. A., Hare T. M., Schelble R. T., Sutherland V. A., and Feldman W. C. (2003) Paleolakes and impact basins in southern Arabia Terra, including Meridiani Planum: Implications for the formation of hematite deposits on Mars. *J. Geophys. Res.—Planet* **108**, 8075.

Nygren M. A., Gay D. H., and Catlow C. R. A. (1997) Hydroxylation of the surface of the corundum basal plane. *Surf. Sci.* **380**, 113–123.

Ohtani E., Hirao N., Kondo T., Ito M., and Kikegawa T. (2005) Iron-water reaction at high pressure and temperature, and

hydrogen transport into the core. *Phys. Chem. Miner.* **32**, 77–82.

Parise J. B., Marshall W. G., Smith R. I., Lutz H. D., and Möller (2000). *Am. Mineral.* **85**, 189–193.

Parker S. C., de Leeuw N. H., and Redfern S. E. (1999) Atomistic simulation of oxide surfaces and their reactivity with water. *Faraday Discuss.* **114**, 381–393.

Parker S. C., Kelsey E. T., Oliver P. M., and Titiloye J. O. (1993) Computer modelling of inorganic solids and surfaces. *Faraday Discuss.* **95**, 75–84.

Parker S. C., Price G. D., and Leslie M. (1987) The lattice-dynamics and thermodynamics of the Mg_2SiO_4 polymorphs. *Phys. Chem. Miner.* **15**, 181–190.

Parry D. E. (1975) Electrostatic potential in surface region of an ionic-crystal. *Surf. Sci.* **49**, 433–440.

Parry D. E. (1976). *Correction. Surf. Sci.* **54**, 195.

Robbins E. I., and Iberall A. S. (1991) Mineral remains of early life on Earth—on Mars. *Geomicrobiol. J.* **9**, 51–66.

Rohr F., Baumer M., Freund H. J., Mejias J. A., Staemmler V., Muller S., Hammer L., and Heinz K. (1997) Strong relaxations at the Cr_2O_3(0001) surface as determined via low-energy electron diffraction and molecular dynamics simulations. *Surf. Sci.* **372**, L291–L297.

Rosso K. M., and Rustad J. R. (2001) Structures and energies of AlOOH and FeOOH polymorphs from plane wave pseudopotential calculations. *Am. Mineral.* **86**, 312–317.

Rustad J. R., Wasserman E., and Felmy A. R. (1999) Molecular modeling of the surface charging of hematite II. Optimal proton distribution and simulation of surface charge versus pH relationships. *Surf. Sci.* **424**, 28–35.

Schröder K. P., Sauer J., Leslie M., Catlow C. R. A., and Thomas J. M. (1992) Bridging hydroxyl-groups in zeolitic catalysts – a computer-simulation of their structure, vibrational properties and acidity in protonated faujasites (H-Y zeolites). *Chem. Phys. Lett.* **188**, 320–325.

Schwertmann U., and Cornell R. M. (2000) Iron Oxides in the Laboratory. *second ed.* Wiley-VCH.

Shroll R. M., and Straatsma T. P. (2003) Molecular dynamics simulations of the goethite–water interface. *Mol. Simul.* **29**, 1–11.

Soper A. K., and Phillips M. G. (1986). *Chem. Phys.* **107**, 47.

Stipp S. L. S., Hansen M., Kristensen R., Hochella, Jr., M. F., Bennedsen L., Dideriksen K., Balic-Zunic T., Léonard D., and Mathieu H.-J. (2002) Behaviour of Fe-oxides relevant to contaminant uptake in the environment. *Chem. Geol.* **190**, 321–337.

Suber L., Imperatori P., Ausanio G., Fabbri F., and Hofmeister H. (2005) Synthesis, morphology, and magnetic characterization of iron oxide nanowires and nanotubes. *J. Phys. Chem. B* **109**, 7103–7109.

Tasker P. W. (1979) Surface energies, surface tensions and surface-structure of the alkali-halide crystals. *Philos. Mag. A* **39**, 119–136.

Taylor M. B., Sims C. E., Barrera G. D., and Allan N. L. (1999) Quasiharmonic free energy and derivatives for slabs: oxide surfaces at elevated temperatures. *Phys. Rev. B* **59**, 6742–6751.

Thevuthasan S., Kim Y. J., Yi S. I., Chambers S. A., Morais J., Denecke R., Fadley C. S., Liu P., Kendelewicz T., and Brown, Jr., G. E. (1999) Surface structure of MBE-grown a-Fe2O3 (0001) by intermediate-energy X-ray photoelectron diffraction. *Surf. Sci.* **425**, 276–286.

Titiloye J. O., Parker S. C., and Mann S. (1993). *J. Cryst. Growth* **131**, 533.

Trainor T. P., Chaka A. M., Eng P. J., Newville M., Waychunas G. G., Catalano J. G., and Brown, Jr., G. E. (2004) Structure and reactivity of the hydrated hematite (0001) surface. *Surf. Sci.* **573**, 204–224.

Tronc E., Chaneac C., and Jolivet J. P. (1998) Structural and magnetic characterization of epsilon-Fe_2O_3. *J. Solid State Chem.* **139**, 93–104.

Wang X. G., Weiss W., Shaikhutdinov K., Ritter M., Petersen M., Wagner F., Schlögl R., and Scheffler M. (1998) The hematite (alpha-Fe_2O_3) (0001) surface: evidence for domains of distinct chemistry. *Phys. Rev. Lett.* **81**, 1038–1041.

Wang Z. L. (1992) Atomic step structures on cleaved alpha-alumina (012) surfaces. *Surf. Sci.* **271**, 477–492.

Wasserman E., Rustad J. R., Felmy A. R., Hay B. P., and Halley J. (1997) Ewald methods for polarizable surfaces with application to hydroxylation and hydrogen bonding on the (012) and (001) surfaces of alpha-Fe_2O_3. *Surf. Sci.* **385**, 217–239.

Wasserman E., Rustad J. R., and Felmy A. R. (1999) Molecular modeling of the surface charging of hematite I. The calculation of proton affinities and acidities on a surface. *Surf. Sci.* **424**, 19–27.

Watson G. W., Kelsey E. T., de Leeuw N. H., Harris D. J., and Parker S. C. (1996) Atomistic simulation of dislocations, surfaces and interfaces in MgO. *J. Chem. Soc. Faraday Trans.* **92**, 433–438.

Wulff G. (1901). *Z. Kristallogr. Kristallgeom.* **34**, 949.

Zhang H., and Selim H. M. (2005) Kinetics of arsenate adsorption–desorption in soils. *Environ. Sci. Technol.* **39**, 6101–6108.

Zhukhlistov A. P. (2001) Crystal structure of lepidocrocite FeO(OH) from the electron-diffractometry data. *Crystallogr. Rep.* **46**, 730–733.

Associate editor: Carrick M. Eggleston